June 13, 1996

Toroidal Gyrofluid Equations for Simulations of Tokamak Turbulence

M. A. Beer and G. W. Hammett

Princeton University Plasma Physics Laboratory, Princeton, NJ 08543

Abstract

A set of nonlinear gyrofluid equations for simulations of tokamak turbulence are derived by taking moments of the nonlinear toroidal gyrokinetic equation. The moment hierarchy is closed with approximations that model the kinetic effects of parallel Landau damping, toroidal drift resonances, and finite Larmor radius effects. These equations generalize the work of Dorland and Hammett [Phys. Fluids B **5**, 812 (1993)] to toroidal geometry by including essential toroidal effects. The closures for phase mixing from toroidal ∇B and curvature drifts take the basic form presented in Waltz, *et al.* [Phys. Fluids B **4**, 3138 (1992)], but here a more rigorous procedure is used, including an extension to higher moments, which provides significantly improved accuracy. In addition, trapped ion effects and collisions are incorporated. This reduced set of nonlinear equations accurately models most of the physics considered important for ion dynamics in core tokamak turbulence, and is simple enough to be used in high resolution direct numerical simulations.

PACS numbers: 52.65.Tt, 52.35.Qz, 52.55.Fa, 52.35.Ra

I. Introduction

Fluid equations have long been used to provide a reduced description of plasma dynamics and to carry out paradigm studies of plasma turbulence which have provided much insight.[1–4] This paper builds on previous fluid descriptions by including important kinetic effects necessary for more realistic simulations of plasma turbulence, especially "toroidal" effects arising from variations in the strength of the magnetic field. These toroidal gyrofluid (or gyro-Landau fluid) equations describe the time evolution of a few moments of the gyrokinetic equation. We will concentrate on a set of six guiding center moments: the guiding center density, n, parallel velocity, $u_\parallel$, parallel pressure, $p_\parallel$, perpendicular pressure, $p_\perp$, and the parallel fluxes of parallel and perpendicular heat, $q_\parallel$ and $q_\perp$. The moment hierarchy is closed by approximations which model the kinetic effects of collisionless phase mixing from parallel free streaming[5,6] and toroidal ∇B and curvature drifts,[7,8] and finite Larmor radius (FLR) effects.[9] The toroidal gyrofluid equations presented here incorporate reliable models of most of the physics considered important for electrostatic ion dynamics in tokamak turbulence. This reduced set of nonlinear fluid equations is simple, yet accurate enough to be used in three-dimensional high resolution direct numerical simulations of tokamak turbulence.[7,10] This paper presents the first detailed derivation of the governing equations used in the toroidal gyrofluid simulations of Refs. 11, 12, and 13.

Toroidal ∇B and curvature drift effects are an important destabilization mechanism for tokamak microinstabilities. The growth rates for the toroidal ion temperature gradient (ITG) driven mode are typically two to three times higher than the growth rates of the slab ITG mode, and toroidicity changes the character of the instability: in a sheared slab the instability is a modified ion sound wave, in a torus it is more interchange-like. In addition, nonlinear simulations of toroidal ITG turbulence find much larger fluctuation and transport levels than sheared slab simulations for the same parameters, bringing the predicted ion heat flux up to experimentally measured levels.[7,10] Thus, incorporating toroidal effects is essential. The key difficulty here is closing the higher moments

introduced by the velocity dependence of the toroidal ∇B and curvature drifts. We close these terms with closure approximations similar in spirit to Ref. 8, but here we use a more rigorous procedure to find our closure coefficients, providing significantly improved accuracy. The derivation presented here is valid for finite $k_\parallel$, while Ref. 8 focused on the purely toroidal ($k_\parallel = 0$) limit and a term to remove a singularity for finite $k_\parallel$ was added *a posteriori*. In addition to presenting a four moment model (four moments were used in Ref. 8), we have extended our model to evolve six moments, which is significantly more accurate. These toroidal gyrofluid equations also incorporate linear and nonlinear FLR effects as in Ref. 9, although the linear FLR terms are modified by toroidicity.

Another important toroidal effect is the damping of poloidal flows. Slab[14,15] and toroidal[16,11] gyrofluid simulations revealed that an important nonlinear saturation process for core tokamak turbulence is the nonlinear generation and damping of radially sheared "zonal" $\mathbf{E} \times \mathbf{B}$ flows: flows which cause flux surfaces to rotate. These sheared flows are very weakly damped in a sheared slab via classical viscosity; the dominant damping mechanisms arise from toroidal effects. The fluid terms arising from the mirroring $\mu \hat{\mathbf{b}} \cdot \nabla B$ and toroidal drift terms in the gyrokinetic equation are included to provide accurate models of poloidal flow damping from magnetic pumping. These mirroring terms also model the effects of trapped ions, extending the validity of these equations into the trapped ion regime at low $k_\theta \rho_i$. Finally, a Krook collision operator has been incorporated, important for poloidal flow damping in the Pfirsch-Schlüter regime, and for collisional effects on very low frequency modes.

We begin by reducing the toroidal gyrokinetic equation to a convenient form in Sec. II; then exact moment equations are derived in Sec. III. Finite Larmor radius effects are treated in Sec. IV. The kinetic linear response function is derived in Sec. V and used to optimize the closure approximations in Sec. VI. The final equations are presented in Sec. VII. A simpler and slightly less accurate set of equations evolving four moments is given in Sec. VIII. These equations are thoroughly tested against fully kinetic linear theory in Sec. IX. Finally, a summary of these results is given in Sec. X, and we discuss the validity of these equations for nonlinear simulations of tokamak

turbulence.

II. The Toroidal Gyrokinetic Equation

The starting point of the derivation of the toroidal ion gyrofluid equations is the nonlinear electrostatic gyrokinetic equation in toroidal geometry,[17,18] also see Refs. 19–21. Our fluid equations are therefore based on the usual gyrokinetic ordering:

$$\frac{\omega}{\Omega} \sim \frac{k_\parallel v_t}{\Omega} \sim \frac{e\Phi}{T} \sim \frac{F_1}{F_0} \sim \frac{\rho}{L} \sim \varepsilon \ll 1, \qquad\qquad k_\perp \rho \sim 1, \tag{1}$$

where ω is a typical frequency, $\Omega = eB/mc$ is the cyclotron frequency, $k_\parallel$ is a typical parallel wavenumber, $k_\perp$ is a typical perpendicular wavenumber, $\rho = v_t/\Omega$ is the gyroradius, $v_t^2 = T/m$ is the thermal velocity, and L is a macroscopic equilibrium scale length, e.g. the density scale length $L_n^{-1} = -(1/n_0)\nabla n_0$. Although we will usually omit the species index, the equations derived in this paper will apply to any ion species, for which $k_\perp \rho \sim 1$ and $\omega \sim \omega_t = v_t/qR$: main ions, impurities, or a Maxwellian energetic component (e.g., beam ions). The ordering $k_\perp \rho \sim 1$ is a "maximal ordering" and allows for a subsidiary expansion $k_\perp \rho \ll 1$ at a later time, although we will assume that $k_\perp$ isn't too small, i.e., we will assume $k_\perp L \gg 1$. The gyrokinetic equations, at least the version we are presently using, may need a generalization to be able to handle the plasma edge where equilibrium gradients may be short enough that $k_\perp L \sim 1$ and $e\Phi/T \sim 1$. The gyrokinetic ordering removes the fast cyclotron time scale by averaging over the gyroangle, reducing the velocity space dimensions from three to two. It also retains the physics of strong turbulence even though the fluctuating quantities $e\Phi/T$ and F_1/F_0 are ordered small, since $\nabla F_1/\nabla F_0 \sim 1$. Thus the dominant $\mathbf{E} \times \mathbf{B}$ nonlinearity is retained, and other nonlinearities are $\mathcal{O}(\varepsilon)$ smaller. In conservative form, the resulting equation is:

$$\begin{aligned} &\frac{\partial}{\partial t} FB + \nabla \cdot \Big[FB(v_\parallel \hat{\mathbf{b}} + \mathbf{v}_E + \mathbf{v}_d) \Big] \\ &+ \frac{\partial}{\partial v_\parallel} \left[FB(-\frac{e}{m} \hat{\mathbf{b}} \cdot \nabla J_0 \Phi - \mu \hat{\mathbf{b}} \cdot \nabla B + v_\parallel (\hat{\mathbf{b}} \cdot \nabla \hat{\mathbf{b}}) \cdot \mathbf{v}_E) \right] = B\, C(F), \end{aligned} \tag{2}$$

which is valid up to $\mathcal{O}(\varepsilon)$. This equation describes the evolution of the gyrophase independent part of the guiding center distribution function $F = F(\mathbf{R}, v_\parallel, \mu, t)$, where $\mu = v_\perp^2/2B$, $v_\parallel$ is the parallel guiding center velocity, and $\mathbf{R}$ is the guiding center position. This form is valid for a general magnetic field, and $\hat{\mathbf{b}}$ is the unit vector in the direction of the magnetic field, $\mathbf{B} = B\hat{\mathbf{b}}$. The combination FB enters because B is the Jacobian of the transformation from $(v_\parallel, v_\perp)$ variables to $(v_\parallel, \mu)$. Because finite Larmor radius effects are retained ($k_\perp \rho \sim 1$), the particles feel the gyroaveraged $\mathbf{E} \times \mathbf{B}$ drift, $\mathbf{v}_E = (c/B)\hat{\mathbf{b}} \times \nabla J_0 \Phi$, where J_0 is the linear operator that carries out the gyroaveraging of the electrostatic potential. In Fourier space, this operator is the Bessel function $J_0(k_\perp v_\perp/\Omega)$, where $k_\perp$ is the perpendicular wavenumber of Φ, not of F.

Toroidicity enters in Eq. (2) through the ∇B and curvature drifts, the $v_\parallel(\hat{\mathbf{b}} \cdot \nabla \hat{\mathbf{b}}) \cdot \mathbf{v}_E$ toroidal angular momentum conserving term, through the non-zero divergence of $\mathbf{v}_E$ in toroidal geometry, toroidal FLR effects, and the $\mu \hat{\mathbf{b}} \cdot \nabla B$ mirroring force. All these terms arise because B is not constant in general, in contrast to a sheared slab model. In Eq. (2), the ∇B and curvature drifts have been combined in

$$\mathbf{v}_d = \frac{v_\parallel^2}{\Omega} \hat{\mathbf{b}} \times (\hat{\mathbf{b}} \cdot \nabla \hat{\mathbf{b}}) + \frac{\mu}{\Omega} \hat{\mathbf{b}} \times \nabla B. \tag{3}$$

Using the equilibrium relations $\nabla p = (1/c)\mathbf{J} \times \mathbf{B}$ and $(4\pi/c)\mathbf{J} = \nabla \times \mathbf{B}$, and the identity $\hat{\mathbf{b}} \cdot \nabla \hat{\mathbf{b}} = (\nabla \times \hat{\mathbf{b}}) \times \hat{\mathbf{b}}$, this can be written:

$$\mathbf{v}_d = \frac{v_\parallel^2 + \mu B}{\Omega B^2} \mathbf{B} \times \nabla B + \frac{4\pi v_\parallel^2}{\Omega B^2} \hat{\mathbf{b}} \times \nabla p, \tag{4}$$

where the ∇p term is negligible for $\beta = 8\pi p/B^2 \ll 1$. For larger β, or stongly rotating plasmas where $n m_i \mathbf{v} \cdot \nabla \mathbf{v}$ is not ignorable in the equilibrium force balance equation, one simply needs to keep the curvature and ∇B drifts separately. Thus instead of ω_d in Eq. (10), one would use two operators: $\omega_{\nabla B}$ and ω_κ, as in Ref. 22.

For ion species, collisional effects will be modeled with a particle, momentum, and energy

conserving BGK operator[23] (ion-electron collisions are negligible):

$$C(F_j) = -\sum_k \nu_{jk}(F_j - F_{Mjk}), \tag{5}$$

where ν_{jk} is the collision rate of species j with species k. Collisions between species j and k cause F_j to relax to a shifted Maxwellian, F_{Mjk}, with the appropriate density, velocity, and temperature to conserve particles, momentum, and energy. Because F_1 is small, F_{Mjk} can be linearized. For a single ion species plasma, this leads to:

$$C(F) = -\nu_{ii}\left\{F_1 - \left[\frac{n_1}{n_0} + \frac{u_\parallel v_\parallel}{v_t^2} + \frac{T_1}{T_0}\left(\frac{v^2}{2v_t^2} - \frac{3}{2}\right)\right]F_0\right\}, \tag{6}$$

where $v^2 = v_\parallel^2 + v_\perp^2$ and $T_1 = (T_{\parallel 1} + 2T_{\perp 1})/3$. The generalization for multiple ion species can be found in Refs. 23 and 24.

Since the perturbations of interest satisfy $k\lambda_D \ll 1$ ($\lambda_D \ll \rho_i$ for typical tokamak parameters), we will assume quasineutrality, $n_e = \sum Z_j n_j$, where n_e is the electron density, n_j is the ion particle density (not the guiding center density) of the j'th species, and $Z_j e$ is the species charge. The ion particle density is related to the guiding center density by:[19–21]

$$n_j = \bar{n}_j - n_{j0}(1 - \Gamma_0)\frac{Z_j e\Phi}{T_j}, \tag{7}$$

where $\Gamma_0(b_j) = \exp(-b_j)I_0(b_j)$, I_0 is a modified Bessel function, $b_j = k_\perp^2 v_{t\perp j}^2/\Omega_j^2 = k_\perp^2\rho_j^2$, and $v_{t\perp j}^2 = T_{\perp j}/m_j$. The second term on the right hand side of Eq. (7) arises from the gyrophase *dependent* part of the distribution function, and is usually called the polarization density. The $k_\perp$ in the polarization density term is from Φ. The contribution to the particle density from the gyrophase *independent* part of the distribution function, $\bar{n}_j$, is

$$\bar{n}_j = \int d^3v\, J_0 F = \int d^3v\, (F_0 + J_0 F_1). \tag{8}$$

Here J_0 operates on F_1, i.e. $k_\perp$ comes from F_1. For a pure ion-electron plasma, with hydrogenic ions ($Z = 1$), the quasineutrality constraint simplifies to:

$$n_e = \bar{n}_i - n_{i0}(1 - \Gamma_0)\frac{e\Phi}{T_i}, \tag{9}$$

For simpler notation, in the remainder of this paper we we will drop the species index j and set $Z_j = 1$. To incorporate multiple ion species, one simply evolves the moments for each species independently. Different species are coupled together through the quasineutrality constraint and through interspecies collision terms.

We will now manipulate Eq. (2) into a form convenient for deriving fluid equations. All of the toroidal effects except the $\mu\hat{\mathbf{b}} \cdot \nabla B$ terms can be written compactly using the notation:

$$i\omega_d \equiv (v_t^2/\Omega B^2)\mathbf{B} \times \nabla B \cdot \nabla. \tag{10}$$

Let us first look at the ∇B and curvature drift terms. For example, pulling $(\Omega B^2)^{-1}\mathbf{B} \times \nabla B$ out of the divergence:

$$\nabla \cdot [FB\mathbf{v}_d] = \frac{1}{\Omega B^2}\mathbf{B} \times \nabla B \cdot \nabla[FB(v_\parallel^2 + \mu B)] + FB(v_\parallel^2 + \mu B)\nabla \cdot \left[\frac{1}{\Omega B^2}\mathbf{B} \times \nabla B\right],$$

the second term becomes:

$$\nabla \cdot \left[\frac{1}{\Omega B^2}\mathbf{B} \times \nabla B\right] = \frac{1}{\Omega B^2}\nabla B \cdot \nabla \times \mathbf{B} \simeq 0$$

which is small for low β since the toroidal component of ∇B is zero and the current, $\mathbf{J}$, is mostly toroidal. Thus, for low β:

$$\nabla \cdot (FB\mathbf{v}_d) = \frac{1}{\Omega B^2}\mathbf{B} \times \nabla B \cdot \nabla[FB(v_\parallel^2 + \mu B)] = (1/v_t^2)i\omega_d[FB(v_\parallel^2 + \mu B)]. \tag{11}$$

In toroidal geometry, FLR effects are complicated by the fact that the argument of J_0 depends on B. When deriving fluid equations by taking moments of Eq. (2), it is easiest if F and J_0 appear together, i.e. on the same side of spatial gradient operators. We now manipulate the terms in Eq. (2) involving $J_0\Phi$ so gradients only act on the combination FJ_0 or FJ_1. Defining $\alpha = k_\perp v_\perp/\Omega$, and recalling that the spatial gradients are taken holding $v_\parallel$ and μ fixed, we can write:

$$\nabla J_0\Phi = J_0\nabla\Phi + \Phi\nabla J_0,$$

$$\nabla J_0(k_\perp v_\perp/\Omega) = \nabla J_0(\alpha) = \frac{\partial J_0}{\partial \alpha}\nabla\alpha = J_1(\alpha)\frac{\alpha}{2B}\nabla B.$$

The $\mathbf{E}\times\mathbf{B}$ term becomes:

$$\nabla\cdot[FB\mathbf{v}_E]=\nabla\cdot[FBJ_0\frac{c}{B^2}\mathbf{B}\times\nabla\Phi+FB\Phi J_1\frac{\alpha}{2B}\frac{c}{B^2}\mathbf{B}\times\nabla B].$$

The divergence of the $\mathbf{E}\times\mathbf{B}$ drift can be written in the same form as the ∇B and curvature drift terms:

$$\nabla\cdot[\frac{c}{B^2}\mathbf{B}\times\nabla\Phi]=\frac{c}{B^2}\nabla\Phi\times(\nabla\times\mathbf{B})-\frac{2c}{B^3}(\mathbf{B}\times\nabla\Phi)\cdot\nabla B\simeq 2(e/T)i\omega_d\Phi,$$

since again, $\nabla\Phi$ is mostly perpendicular, and $\mathbf{J}$ is mostly toroidal. Writing $\mathbf{v}_\Phi=(c/B)\hat{\mathbf{b}}\times\nabla\Phi$, we have:

$$\nabla\cdot[FB\mathbf{v}_E]=\mathbf{v}_\Phi\cdot\nabla(FBJ_0)+2FBJ_0(e/T)i\omega_d\Phi+(e/T)i\omega_d(FBJ_1\Phi\frac{k_\perp v_\perp}{2\Omega}).$$

The first term on the RHS includes the usual linear ω_* terms from F_0 and the $\mathbf{E}\times\mathbf{B}$ nonlinearity from F_1, with FLR corrections as discussed in Ref. 9. The linear pieces of the second and third toroidal terms ($\propto F_0$) are of the same order as the slab $\mathbf{E}\times\mathbf{B}$ nonlinearity in the gyrokinetic ordering (we keep $B^{-1}\nabla B\sim F_0^{-1}\nabla F_0$). The nonlinear pieces in the toroidal terms ($\propto F_1$) are higher order in the gyrokinetic ordering, and can be ignored.

Performing similar manipulations on the toroidal angular momentum conserving term, using the identity $(\hat{\mathbf{b}}\cdot\nabla\hat{\mathbf{b}})\cdot\mathbf{v}_E=-(c/B^3)(\mathbf{B}\times\nabla B)\cdot\nabla J_0\Phi$, leads to:

$$\begin{aligned}\frac{\partial}{\partial v_\parallel}[FBv_\parallel(\hat{\mathbf{b}}\cdot\nabla\hat{\mathbf{b}})\cdot\mathbf{v}_E] &= -\frac{\partial}{\partial v_\parallel}(Fv_\parallel)\frac{c}{B^2}\mathbf{B}\times\nabla B\cdot\nabla J_0\Phi\\ &= -\frac{\partial}{\partial v_\parallel}(Fv_\parallel)\frac{c}{B^2}\mathbf{B}\times\nabla B\cdot(J_0\nabla\Phi+J_1\frac{\alpha}{2B}\nabla B).\end{aligned}$$

The J_0 term again has the ω_d form, and the J_1 term vanishes leaving:

$$\frac{\partial}{\partial v_\parallel}[FBv_\parallel(\hat{\mathbf{b}}\cdot\nabla\hat{\mathbf{b}})\cdot\mathbf{v}_E]=-\frac{\partial}{\partial v_\parallel}(FBJ_0v_\parallel)(e/T)i\omega_d\Phi.$$

Since $k_\parallel\rho\sim\varepsilon$, the only contribution from the $E_\parallel$ term is linear, so in this term we only need F_0. Using the notation $\nabla_\parallel=\hat{\mathbf{b}}\cdot\nabla$, and a Maxwellian F_0:

$$F_0=\frac{n_0}{(2\pi v_t^2)^{3/2}}e^{-v_\parallel^2/2v_t^2-\mu B/v_t^2},\tag{12}$$

we have $\nabla_\parallel|_{v_\parallel,\mu} B(\partial F_0/\partial v_\parallel) = (\partial F_0/\partial v_\parallel)B(1-\mu B/v_t^2)\nabla_\parallel \ln B$, so this term becomes:

$$-\frac{e}{m}(\hat{\mathbf{b}}\cdot\nabla J_0\Phi)\frac{\partial F_0}{\partial v_\parallel}B = -\frac{e}{m}\nabla_\parallel(J_0\Phi B\frac{\partial F_0}{\partial v_\parallel}) + \frac{e}{m}J_0\Phi B\frac{\partial F_0}{\partial v_\parallel}(\mu B/v_t^2-1)\nabla_\parallel \ln B.$$

Combining all these terms, Eq. (2) can be written:

$$\begin{aligned}\frac{\partial}{\partial t}FB &+ B\nabla_\parallel\frac{FBv_\parallel}{B} + \mathbf{v}_\Phi\cdot\nabla(FBJ_0) + 2FBJ_0(e/T)i\omega_d\Phi \\ &+ (e/T)i\omega_d(FBJ_1\Phi k_\perp v_\perp/2\Omega) + \frac{i\omega_d}{v_t^2}[FB(v_\parallel^2+\mu B)] - \frac{e}{m}\nabla_\parallel(J_0\Phi B\frac{\partial F_0}{\partial v_\parallel}) \\ &+ \frac{e}{m}J_0\Phi B\frac{\partial F_0}{\partial v_\parallel}\left(\frac{\mu B}{v_t^2}-1\right)\nabla_\parallel \ln B - \mu B\frac{\partial}{\partial v_\parallel}(FB)\nabla_\parallel \ln B \\ &- \frac{\partial}{\partial v_\parallel}(FBJ_0v_\parallel)(e/T)i\omega_d\Phi = 0.\end{aligned} \tag{13}$$

This form is messy, but most suited for taking moments, because velocity dependent terms such as F, J_0, μ, etc., are grouped together on the same side of spatial gradient operators.

III. General Toroidal Gyrofluid Equations

We are interested in deriving evolution equations for velocity space moments of Eq. (13), defined by:

$$\begin{array}{cc} n = \int F\, d^3v & n u_\parallel = \int F v_\parallel\, d^3v \\ p_\parallel = m\int F(v_\parallel-u_\parallel)^2\, d^3v & p_\perp = (m/2)\int F v_\perp^2\, d^3v \\ q_\parallel = m\int F(v_\parallel-u_\parallel)^3\, d^3v & q_\perp = (m/2)\int F v_\perp^2(v_\parallel-u_\parallel)\, d^3v \\ r_{\parallel,\parallel} = m\int F(v_\parallel-u_\parallel)^4\, d^3v & r_{\parallel,\perp} = (m/2)\int F v_\perp^2(v_\parallel-u_\parallel)^2\, d^3v \\ r_{\perp,\perp} = (m/4)\int F v_\perp^4\, d^3v & s_{\perp,\perp} = (m/4)\int F(v_\parallel-u_\parallel)v_\perp^4 d^3v \\ s_{\parallel,\parallel} = m\int F(v_\parallel-u_\parallel)^5 d^3v & s_{\parallel,\perp} = (m/2)\int F(v_\parallel-u_\parallel)^3 v_\perp^2 d^3v \end{array}$$

It will often be convenient to use temperature instead of pressure, where the parallel temperature is defined by $p_\parallel \equiv nT_\parallel$ and perpendicular temperature by $p_\perp \equiv nT_\perp$

We now proceed to derive moment equations by integrating Eq. (13) over velocity space. These equations express exact conservation laws of the gyrokinetic equation in the collisionless limit: conservation of particles, momentum, etc. However, because of the velocity dependence in the parallel free streaming term, $k_\parallel v_\parallel$, the toroidal drift terms, $\omega_d(v_\parallel^2+v_\perp^2/2)$, the mirroring terms $v_\perp^2\nabla\ln B$, and the FLR terms, $J_0(k_\perp v_\perp/\Omega)$, higher moments are introduced into each of these

equations, leading to the usual problem of the coupled moments hierarchy. These equations are not useful until closure approximations are made for the highest moments that are not evolved, as discussed in following sections. Taking integrals of the form $\int dv_\parallel d\mu\, v_\parallel^j \mu^k \ldots$ of Eq. (13) leads to the following exact moment equations, using the notation: $n\langle A\rangle = \int d^3v\, FA = 2\pi \int dv_\parallel d\mu\, FBA$:

$$\begin{aligned}\frac{\partial n}{\partial t} &+ B\nabla_\parallel(nu_\parallel/B) + \mathbf{v}_\Phi\cdot\nabla(n\langle J_0\rangle) + 2n\langle J_0\rangle(e/T)i\omega_d\Phi \\ &+ (e/T)i\omega_d(\Phi n\langle J_1\alpha\rangle/2) + (1/T)i\omega_d(p_\parallel + p_\perp + nmu_\parallel^2) = 0,\end{aligned} \tag{14}$$

$$\begin{aligned}\frac{\partial}{\partial t}nu_\parallel &+ B\nabla_\parallel(p_\parallel/m + nu_\parallel^2)/B + \mathbf{v}_\Phi\cdot\nabla(n\langle J_0 v_\parallel\rangle) + 2n\langle J_0 v_\parallel\rangle(e/T)i\omega_d\Phi \\ &+ (e/T)i\omega_d(\Phi n\langle J_1 v_\parallel\alpha\rangle/2) + (1/T)i\omega_d(q_\parallel + q_\perp + 3p_\parallel u_\parallel + p_\perp u_\parallel + nmu_\parallel^3) \\ &+ \frac{e}{m}\nabla_\parallel n\langle J_0\rangle\Phi + \frac{e}{m}n\langle J_0(v_\perp^2/2v_t^2 - 1)\rangle\Phi\nabla_\parallel \ln B + \frac{p_\perp}{m}\nabla_\parallel \ln B \\ &+ n\langle J_0 v_\parallel\rangle(e/T)i\omega_d\Phi = 0,\end{aligned} \tag{15}$$

$$\begin{aligned}\frac{\partial}{\partial t}(p_\parallel + nmu_\parallel^2) &+ B\nabla_\parallel(q_\parallel + 3p_\parallel u_\parallel + nmu_\parallel^2)/B + \mathbf{v}_\Phi\cdot\nabla(n\langle J_0 v_\parallel^2\rangle) \\ &+ 2n\langle J_0 v_\parallel^2\rangle(e/T)i\omega_d\Phi + (e/T)i\omega_d(\Phi n\langle J_1 v_\parallel^2\alpha\rangle/2) \\ &+ (1/T)i\omega_d(r_{\parallel,\parallel} + r_{\parallel,\perp} + 4q_\parallel u_\parallel + q_\perp u_\parallel + 6p_\parallel u_\parallel^2 + p_\perp u_\parallel^2 + nmu_\parallel^4) \\ &+ 2\frac{e}{m}\nabla_\parallel n\langle J_0 v_\parallel\rangle\Phi + 2\frac{e}{m}n\langle J_0 v_\parallel(v_\perp^2/2v_t^2 - 1)\rangle\Phi\nabla_\parallel \ln B \\ &+ 2(q_\perp + p_\perp u_\parallel)\nabla_\parallel \ln B + 2n\langle J_0 v_\parallel^2\rangle(e/T)i\omega_d\Phi = 0,\end{aligned} \tag{16}$$

$$\begin{aligned}\frac{\partial}{\partial t}\frac{p_\perp}{B} &+ B\nabla_\parallel(q_\perp + p_\perp u_\parallel)/B^2 + \mathbf{v}_\Phi\cdot\nabla\frac{n\langle J_0 v_\perp^2\rangle}{2B} + 2\frac{n\langle J_0 v_\perp^2\rangle}{2B}(e/T)i\omega_d\Phi \\ &+ (e/T)i\omega_d(\Phi n\langle J_1 v_\perp^2\alpha\rangle/4B) + (1/T)i\omega_d(r_{\parallel,\perp} + r_{\perp,\perp} + q_\perp u_\parallel + p_\perp u_\parallel^2)/B = 0,\end{aligned} \tag{17}$$

$$\begin{aligned}&\frac{\partial}{\partial t}(q_\parallel + 3p_\parallel u_\parallel + nmu_\parallel^2) + B\nabla_\parallel(r_{\parallel,\parallel} + 4q_\parallel u_\parallel + 6p_\parallel u_\parallel^2 + nmu_\parallel^4)/B \\ &+ \mathbf{v}_\Phi\cdot\nabla(n\langle J_0 v_\parallel^3\rangle) + 2n\langle J_0 v_\parallel^3\rangle(e/T)i\omega_d\Phi + (e/T)i\omega_d(\Phi n\langle J_1 v_\parallel^3\alpha\rangle/2) \\ &+ (1/T)i\omega_d(s_{\parallel,\parallel} + s_{\parallel,\perp} + 5r_{\parallel,\parallel}u_\parallel + 3r_{\parallel,\perp}u_\parallel + 10q_\parallel u_\parallel^2 + 10p_\parallel u_\parallel^3 + p_\perp u_\parallel^3 + nmu_\parallel^5) \\ &+ 3\frac{e}{m}\nabla_\parallel n\langle J_0 v_\parallel^2\rangle\Phi + 3\frac{e}{m}n\langle J_0 v_\parallel^2(v_\perp^2/2v_t^2 - 1)\rangle\Phi\nabla_\parallel \ln B \\ &+ 3(r_{\parallel,\perp} + 2q_\perp u_\parallel + p_\perp u_\parallel^2)\nabla_\parallel \ln B + 3n\langle J_0 v_\parallel^3\rangle(e/T)i\omega_d\Phi = 0,\end{aligned} \tag{18}$$

$$\frac{\partial}{\partial t}\frac{q_\perp + p_\perp u_\parallel}{B} + B\nabla_\parallel (r_{\parallel,\perp} + 2q_\perp u_\parallel + p_\perp u_\parallel^2)/B^2 + \mathbf{v}_\Phi \cdot \nabla \frac{n\langle J_0 v_\parallel v_\perp^2\rangle}{2B} \tag{19}$$

$$+ \quad 2\frac{n\langle J_0 m v_\parallel v_\perp^2\rangle}{2B}(e/T)i\omega_d\Phi + (e/T)i\omega_d(\Phi n\langle J_1 v_\parallel v_\perp^2 \alpha\rangle/4B)$$

$$+ \quad (1/T)i\omega_d(s_{\parallel,\perp} + s_{\perp,\perp} + 3r_{\parallel,\perp}u_\parallel + r_{\perp,\perp}u_\parallel + p_\perp u_\parallel^3)/B + \frac{e}{m}\nabla_\parallel \frac{n\langle J_0 v_\perp^2\rangle\Phi}{2B}$$

$$+ \quad \frac{e}{m} n\langle J_0(v_\perp^2/2B)(v_\perp^2/2v_t^2 - 1)\rangle \Phi \nabla_\parallel \ln B$$

$$+ \quad \frac{r_{\perp,\perp}}{B}\nabla_\parallel \ln B + n\langle J_0 v_\parallel v_\perp^2/B\rangle(e/T)i\omega_d\Phi = 0.$$

Before proceeding to discuss closure approximations, it is useful to note that many of these terms are higher order in the gyrokinetic ordering, and can be neglected. By separating the moments into equilibrium and fluctuating parts the parallel nonlinearities drop out, since they are higher order in ε. For example, we let $n = n_0 + n_1$, where $n_1/n_0 \sim \mathcal{O}(\varepsilon)$. We retain the dominant $\mathbf{E}\times\mathbf{B}$ nonlinearities (the $\mathbf{v}_\Phi\cdot\nabla$ terms), which are leading order. In addition, we assume F_0 is an unshifted Maxwellian, so the equilibrium parts of odd moments are zero, and terms like $u_\parallel^2$ are higher order in ε.

IV. Finite Larmor Radius Effects

In Ref. 9, accurate models of FLR effects were developed by carefully approximating velocity space averages of J_0 which appear in the dynamical equations and in the quasineutrality constraint, Eq. (9). As in Ref. 9, we choose to evolve moments of the guiding center distribution function, not real space moments, to provide a better description of linear FLR effects including the "Bakshi-Linsker" effect,[25,26] and additional FLR nonlinearities. For simplicity, we will not incorporate the nonlinear FLR phase mixing model in Ref. 9, specifically because in our toroidal nonlinear simulations we do not see large fluctuation levels at high $k_\perp\rho_i$, where these terms become important. In addition to approximating $\langle J_0\rangle$, $\langle J_0 v_\parallel\rangle$, $\langle J_0 v_\parallel^2\rangle$, $\langle J_0 v_\perp^2\rangle$, $\langle J_0 v_\parallel^3\rangle$, and $\langle J_0 v_\parallel v_\perp^2\rangle$, which appear in the slab limit, we also need to approximate $\langle J_0 v_\perp^4\rangle$, $\langle J_1\alpha\rangle$, $\langle J_1 v_\parallel^2\alpha\rangle$, and $\langle J_1 v_\perp^2\alpha\rangle$, which arise from toroidal terms. Linearly, these terms involve only F_0, and could be evaluated exactly. However, in

the quasineutrality constraint we have to approximate $\bar{n}_i$, which comes from F_1, see Eq. (8). F_1 is not Maxwellian in general, so the $\langle J_0 F_1 \rangle$ term in $\bar{n}_i$ needs to be approximated. As discussed in Ref. 9, the best agreement with linear kinetic theory is obtained by approximating both the $\langle J_0 \rangle$ terms and $\bar{n}_i$. In the linear kinetic equation, the J_0 in Eq. (8) combines with the J_0 in the $\mathbf{E} \times \mathbf{B}$ drifts in the gyrokinetic equation, Eq. (2), so the average of J_0^2 over a Maxwellian enters the dispersion relation in the slab limit, not the average of J_0. These are quite different, especially for large b, since $\langle J_0^2 \rangle = \Gamma_0(b)$ and $\langle J_0 \rangle^2 = \exp(-b)$. This motivated the $\langle J_0^2 \rangle \approx \Gamma_0^{1/2}$ approximation introduced in Ref. 9, which is more robust and more accurate for linear dispersion relations. With the inclusion of toroidal effects, the $v_\perp$ in $J_0(k_\perp v_\perp/\Omega)$ couples with the $v_\perp^2$ in the toroidal drifts, so it is no longer simply $\Gamma_0(b)$ that enters the linear kinetic equation, see Eq. (52) and Eq. (58). We have not found a completely satisfying replacement to $\langle J_0 \rangle \approx \Gamma_0^{1/2}$ for the general toroidal case, but $\langle J_0 \rangle \approx \Gamma_0^{1/2}$ continues to work reasonably well. Therefore, we will use the results of Ref. 9 to approximate:

$$\langle J_0 \rangle = \Gamma_0^{1/2}, \tag{20}$$

$$\langle J_0 v_\parallel \rangle = v_t \Gamma_0^{1/2}, \tag{21}$$

$$\langle J_0 v_\parallel^2 \rangle = v_t^2 \Gamma_0^{1/2}, \tag{22}$$

$$\langle J_0 v_\perp^2 \rangle = 2 v_t^2 \frac{\partial}{\partial b}(b \Gamma_0^{1/2}) = v_t^2 (2\Gamma_0^{1/2} + \hat{\nabla}_\perp^2) \tag{23}$$

$$\langle J_0 v_\parallel^3 \rangle = v_t^3 \Gamma_0^{1/2}, \tag{24}$$

$$\langle J_0 v_\parallel v_\perp^2 \rangle = 2 v_t^3 \frac{\partial}{\partial b}(b \Gamma_0^{1/2}) = v_t^3 (2\Gamma_0^{1/2} + \hat{\nabla}_\perp^2). \tag{25}$$

The modified Laplacian operators $\hat{\nabla}_\perp^2$ and $\hat{\hat{\nabla}}_\perp^2$ are defined by:

$$\frac{1}{2} \hat{\nabla}_\perp^2 \Psi = b \frac{\partial \Gamma_0^{1/2}}{\partial b} \Phi, \tag{26}$$

$$\hat{\hat{\nabla}}_\perp^2 \Psi = b \frac{\partial^2}{\partial b^2}(b \Gamma_0^{1/2}) \Phi, \tag{27}$$

where $\Psi = \Gamma_0^{1/2} \Phi$ is the approximation to the gyroaveraged potential.

There are four new terms due to toroidicity that need approximating: $\langle J_0 v_\perp^4 \rangle$, $\langle J_1 \alpha \rangle$, $\langle J_1 v_\parallel^2 \alpha \rangle$, and $\langle J_1 v_\perp^2 \alpha \rangle$. Several techniques could be used to approximate these terms; one is to follow the approach and rationale in Ref. 9. For example, the $\langle J_1 \alpha \rangle$ term can be rewritten using the following trick:

$$\langle J_1 \alpha \rangle \approx - \left. \frac{\partial}{\partial \beta} \right|_{\beta=1} \langle J_0(\beta \alpha) \rangle \, . \tag{28}$$

Thus the approximation for $\langle J_0 \rangle$ is the fundamental one, and all other FLR terms can be derived from it. Using $\langle J_0 \rangle \approx \Gamma_0^{1/2}$ leads to:

$$\langle J_1 \alpha \rangle \approx - \left. \frac{\partial}{\partial \beta} \right|_{\beta=1} \Gamma_0^{1/2}(\beta^2 b) = -2b \frac{\partial \Gamma_0^{1/2}}{\partial b} = -\hat{\nabla}_\perp^2, \tag{29}$$

and

$$\left\langle J_1 v_\parallel^2 \alpha \right\rangle \approx -2 v_t^2 b \frac{\partial \Gamma_0^{1/2}}{\partial b} = -v_t^2 \hat{\nabla}_\perp^2. \tag{30}$$

For the $\langle J_1 v_\perp^2 \alpha \rangle$ term, we will assume that F is approximately Maxwellian, so that $v_\perp^2 F \approx 2 v_t^2 \partial (T_\perp F)/\partial T_\perp$, and:

$$\left\langle J_1 v_\perp^2 \alpha \right\rangle \approx - \left. \frac{\partial}{\partial \beta} \right|_{\beta=1} 2 v_t^2 \frac{\partial}{\partial T_\perp} \left(T_\perp \langle J_0(\beta \alpha) \rangle \right) = -4 v_t^2 \frac{\partial}{\partial b} \left(b^2 \frac{\partial \Gamma_0^{1/2}}{\partial b} \right) = -4 v_t^2 \hat{\hat{\nabla}}_\perp^2. \tag{31}$$

The final toroidal FLR term is:

$$\langle J_0 v_\perp^4 \rangle \approx 4 v_t^4 \left[b \frac{\partial^2}{\partial b^2} (b \Gamma_0^{1/2}) + 2b \frac{\partial}{\partial b} (b \Gamma_0^{1/2}) \right] = 4 v_t^4 \left(2 \Gamma_0^{1/2} + \hat{\nabla}_\perp^2 + \hat{\hat{\nabla}}_\perp^2 \right). \tag{32}$$

These approximations remain first order accurate in b to those obtained using the Taylor series expansion $J_0 \approx 1 - k_\perp^2 v_\perp^2 / 4\Omega^2$.

Now we look at linear FLR effects in the $\mathbf{E} \times \mathbf{B}$ terms. For example, in the density equation, following Ref. 9:

$$\mathbf{v}_\Phi \cdot \nabla n \langle J_0 \rangle \simeq \mathbf{v}_\Phi \cdot \nabla (n_0 \Gamma_0^{1/2}) + \text{nonlinear terms} \tag{33}$$

Since $b = k_\perp^2 v_{t\perp}^2 / \Omega^2$ depends on both B and $T_\perp$ (through $v_{t\perp}^2 = T_{\perp 0}/m$), gradients acting on functions of b (FLR modified terms), introduce pieces proportional to ∇B and $\nabla T_{\perp 0}$:

$$\nabla b = \frac{b}{T_{\perp 0}} \nabla T_{\perp 0} - \frac{2b}{B} \nabla B,$$

$$\nabla n_0 \Gamma_0^{1/2} = \Gamma_0^{1/2} \nabla n_0 + n_0 \frac{\partial \Gamma_0^{1/2}}{\partial b} \nabla b.$$

We now introduce the diamagnetic frequency $i\omega_* \equiv -(cT/eBn_0)\nabla n_0 \cdot \hat{\mathbf{b}} \times \nabla$, $\eta_\parallel = L_n/L_{T_\parallel}$, and $\eta_\perp = L_n/L_{T_\perp}$, where $L_{T_\parallel}$ and $L_{T_\perp}$ are the equilibrium scale lengths of parallel and perpendicular temperature, which can be different in general. When they are assumed to be the same, we drop the subscripts, and write η. With these definitions, Eq. (33) becomes:

$$\mathbf{v}_\Phi \cdot \nabla n \langle J_0 \rangle = -n_0 i\omega_* \Gamma_0^{1/2} \frac{e\Phi}{T_0} - n_0 \eta_\perp b \frac{\partial \Gamma_0^{1/2}}{\partial b} i\omega_* \frac{e\Phi}{T_0} + 2n_0 b \frac{\partial \Gamma_0^{1/2}}{\partial b} i\omega_d \frac{e\Phi}{T_0},$$

since $\mathbf{v}_\Phi \cdot (1/B)\nabla B = -i\omega_d(e\Phi/T)$. For a general function of b,

$$\mathbf{v}_\Phi \cdot \nabla n_0 f(b) = -n_0 f(b) i\omega_* \frac{e\Phi}{T_0} - n_0 \eta_\perp b \frac{\partial f}{\partial b} i\omega_* \frac{e\Phi}{T_0} + 2n_0 b \frac{\partial f}{\partial b} i\omega_d \frac{e\Phi}{T_0}.$$

This form will be used to evaluate terms like $\mathbf{v}_\Phi \cdot \nabla \langle n J_0 v_\perp^2 \rangle$.

In the linear part of the $(e/2T) i\omega_d (\Phi n \langle J_1 \alpha \rangle)$ terms, we need to evaluate

$$\omega_d (\Phi n \langle J_1 \alpha \rangle) = n_0 \langle J_1 \alpha \rangle \omega_d \Phi + \Phi n_0 \frac{\partial \langle J_1 \alpha \rangle}{\partial b} \omega_d b + \Phi \langle J_1 \alpha \rangle \omega_d n_0,$$

The last two terms are higher order in ε, so the $\langle J_1 \alpha \rangle$ terms only contribute:

$$(e/2T) i\omega_d (\Phi n \langle J_1 \alpha \rangle) = i n_0 \left\langle J_1 \frac{\alpha}{2} \right\rangle \omega_d \frac{e\Phi}{T_0}.$$

Because the final equations will get rather complicated, for the moment, we will treat the linear and nonlinear terms separately. We normalize time, parallel lengths, and perpendicular lengths as

$$(t, k_\parallel, k_\perp) = (\frac{t v_t}{L_n}, k_\parallel L_n, k_\perp \rho), \tag{34}$$

and fluctuating quantities as

$$\frac{\rho}{L_n}(\Phi, n, u, p, q, r, s) = (\frac{e\Phi}{T_0}, \frac{n_1}{n_0}, \frac{u_1}{v_t}, \frac{p_1}{n_0 m v_t^2}, \frac{q_1}{n_0 m v_t^3}, \frac{r_1}{n_0 m v_t^4}, \frac{s_1}{n_0 m v_t^5}), \tag{35}$$

where normalized quantities are on the left hand side and dimensional quantities are on the right. With these normalizations, the characteristic drift wave time and space scales are $\mathcal{O}(1)$, and the

perturbed quantities will be $\mathcal{O}(1)$ at the gyro-Bohm saturation level. In this paper, all equilibrium quantities are ion parameters, i.e. $T_0 = T_{i0}$, $v_t = v_{ti}$. For the equilibrium F_0 we use a Maxwellian, so the normalized equilibrium values of the moments are $p_{\parallel 0} = 1$, $p_{\perp 0} = 1$, $r_{\parallel,\parallel 0} = 3$, $r_{\parallel,\perp 0} = 1$, and $r_{\perp,\perp 0} = 2$. With the linear FLR approximations discussed above, temporarily ignoring the nonlinear terms, the moment equations, Eqs. (14-19), become:

$$\frac{\partial n}{\partial t} + B\nabla_\parallel \frac{u_\parallel}{B} - \left(1 + \frac{\eta_\perp}{2}\hat{\nabla}_\perp^2\right) i\omega_* \Psi + \left(2 + \frac{1}{2}\hat{\nabla}_\perp^2\right) i\omega_d \Psi + i\omega_d (p_\parallel + p_\perp) = 0, \tag{36}$$

$$\frac{\partial u_\parallel}{\partial t} + B\nabla_\parallel \frac{p_\parallel}{B} + \nabla_\parallel \Psi + \left(p_\perp + \frac{1}{2}\hat{\nabla}_\perp^2 \Psi\right) \nabla_\parallel \ln B + i\omega_d (q_\parallel + q_\perp + 4u_\parallel) = 0, \tag{37}$$

$$\begin{aligned} \frac{\partial p_\parallel}{\partial t} + B\nabla_\parallel \frac{q_\parallel + 3u_\parallel}{B} + 2(q_\perp + u_\parallel)\nabla_\parallel \ln B - \left(1 + \eta_\parallel + \frac{\eta_\perp}{2}\hat{\nabla}_\perp^2\right) i\omega_* \Psi \\ + \left(4 + \frac{1}{2}\hat{\nabla}_\perp^2\right) i\omega_d \Psi + i\omega_d (r_{\parallel,\parallel} + r_{\parallel,\perp}) = 0, \end{aligned} \tag{38}$$

$$\begin{aligned} \frac{\partial p_\perp}{\partial t} + B^2\nabla_\parallel \frac{q_\perp + u_\parallel}{B^2} - \left[1 + \frac{1}{2}\hat{\nabla}_\perp^2 + \eta_\perp \left(1 + \frac{1}{2}\hat{\nabla}_\perp^2 + \hat{\hat{\nabla}}_\perp^{\,2}\right)\right] i\omega_* \Psi \\ + \left(3 + \frac{3}{2}\hat{\nabla}_\perp^2 + \hat{\hat{\nabla}}_\perp^{\,2}\right) i\omega_d \Psi + i\omega_d (r_{\parallel,\perp} + r_{\perp,\perp}) = 0, \end{aligned} \tag{39}$$

$$\begin{aligned} \frac{\partial q_\parallel}{\partial t} + \nabla_\parallel (r_{\parallel,\parallel} - 3p_\parallel) + (-r_{\parallel,\parallel} + 3p_\parallel + 3r_{\parallel,\perp} - 3p_\perp)\nabla_\parallel \ln B \\ + i\omega_d (s_{\parallel,\parallel} + s_{\parallel,\perp} - 3q_\parallel - 3q_\perp + 6u_\parallel) = 0, \end{aligned} \tag{40}$$

$$\begin{aligned} \frac{\partial q_\perp}{\partial t} + \nabla_\parallel \left(r_{\parallel,\perp} - p_\parallel + \frac{1}{2}\hat{\nabla}_\perp^2 \Psi\right) + (-2r_{\parallel,\perp} + r_{\perp,\perp} + p_\parallel - p_\perp)\nabla_\parallel \ln B \\ + \left(\hat{\hat{\nabla}}_\perp^{\,2} \Psi - \frac{1}{2}\hat{\nabla}_\perp^2 \Psi\right) \nabla_\parallel \ln B + i\omega_d (s_{\parallel,\perp} + s_{\perp,\perp} - q_\parallel - q_\perp + u_\parallel) = 0. \end{aligned} \tag{41}$$

If we had evaluated the velocity space averages using a Maxwellian F, giving $\langle J_0 \rangle = \exp(-b)$, the n, $u_\parallel$, $p_\parallel$ and $p_\perp$ equations above would be equivalent to the electrostatic limit of those derived in Ref. 22. The q equations would also be equivalent if Ref. 22 had proceeded to higher moment equations. This equivalence can be verified by replacing $\Gamma_0^{1/2} \to \exp(-b/2)$ and evaluating the derivatives with respect to b in Eqs. (26) and (27). As discussed in the following sections, these equations require closure approximations for $r_{\parallel,\parallel}$, $r_{\parallel,\perp}$, $r_{\perp,\perp}$, $s_{\parallel,\parallel}$, $s_{\parallel,\perp}$, and $s_{\perp,\perp}$, which Ref. 22 did not address.

For the nonlinear terms, we follow Ref. 9. Thus, to each of Eqs. (36-41) we add the usual $\mathbf{E}\times\mathbf{B}$ nonlinearities plus additional FLR nonlinearities, as follows:

$$\frac{\partial n}{\partial t}+\mathbf{v}_\Psi\cdot\nabla n+[\frac{1}{2}\hat{\nabla}_\perp^2\mathbf{v}_\Psi]\cdot\nabla T_\perp+\cdots \tag{42}$$

$$\frac{\partial u_\parallel}{\partial t}+\mathbf{v}_\Psi\cdot\nabla u_\parallel+[\frac{1}{2}\hat{\nabla}_\perp^2\mathbf{v}_\Psi]\cdot\nabla q_\perp+\cdots \tag{43}$$

$$\frac{\partial p_\parallel}{\partial t}+\mathbf{v}_\Psi\cdot\nabla p_\parallel+[\frac{1}{2}\hat{\nabla}_\perp^2\mathbf{v}_\Psi]\cdot\nabla T_\perp+\cdots \tag{44}$$

$$\frac{\partial p_\perp}{\partial t}+\mathbf{v}_\Psi\cdot\nabla p_\perp+[\frac{1}{2}\hat{\nabla}_\perp^2\mathbf{v}_\Psi]\cdot\nabla p_\perp+[\hat{\hat{\nabla}}_\perp^{\,2}\mathbf{v}_\Psi]\cdot\nabla T_\perp+\cdots \tag{45}$$

$$\frac{\partial q_\parallel}{\partial t}+\mathbf{v}_\Psi\cdot\nabla q_\parallel+\cdots \tag{46}$$

$$\frac{\partial q_\perp}{\partial t}+\mathbf{v}_\Psi\cdot\nabla q_\perp+[\frac{1}{2}\hat{\nabla}_\perp^2\mathbf{v}_\Psi]\cdot\nabla u_\parallel+[\hat{\hat{\nabla}}_\perp^{\,2}\mathbf{v}_\Psi]\cdot\nabla q_\perp+\cdots \tag{47}$$

In these terms, $\mathbf{v}_\Psi$ is the approximation to the $\mathbf{E}\times\mathbf{B}$ drift in the gyroaveraged potential, $\mathbf{v}_\Psi=(c/B)\hat{\mathbf{b}}\times\Psi$, where $\Psi=\Gamma_0^{1/2}\Phi$. There is a typographical error in Eq. (59) of Ref. 9, where the nonlinear term involving $q_\perp$ should be dropped.

Now let us return to the quasineutrality constraint, Eq. (9). Here we have to approximate the real space density. Because of the J_0 which acts on F_1, $\bar{n}_i$ will involve the guiding center density and all higher perpendicular moments, but we only evolve up to $T_\perp$. Thus we need another closure approximation which relates $\bar{n}_i$ to n and $T_\perp$. The approximation for $\bar{n}_i$ in Ref. 9 was tailored to fit the local kinetic dispersion relation in the slab limit. In the toroidal case, because of the $v_\perp$ dependence of the toroidal drifts in the resonant denominator of the toroidal response function, Eq. (52), following such a procedure is more complicated, so we simply use

$$\bar{n}_i=\frac{1}{1+b/2}n-\frac{2b}{(2+b)^2}T_\perp. \tag{48}$$

This is first order accurate in b for both the n and $T_\perp$ terms, and behaves appropriately ($\bar{n}_i\to 0$) in the $b\to\infty$ limit. The FLR approximations used here and above provide a reasonably accurate fit to the kinetic FLR behavior in the local kinetic dispersion relation, and continue to perform well nonlocally, as demonstrated in Section IX. The agreement at small b is excellent, and is usually

within 20% for $k_\perp \rho_i \approx 1$. Above $k_\perp \rho_i \approx 1$ the agreement is not as good, but the limiting behavior as $k_\perp \rho_i \to \infty$ is properly recovered. Note that the FLR models described in this section can also be used with a simpler Padé approximation, by substituting $\Gamma_0^{1/2} \to (1 + b/2)^{-1}$ in Eqs. (26) and (27), as discussed in Ref. 9.

V. Local Linear Toroidal Response Function

Our closure approximations for $r_{\parallel,\parallel}$, $r_{\parallel,\perp}$, $r_{\perp,\perp}$, $s_{\parallel,\parallel}$, $s_{\parallel,\perp}$, and $s_{\perp,\perp}$, will be chosen to provide accurate models of the kinetic effects of parallel and toroidal drift phase mixing. Ultimately, we choose the closure coefficients to provide an accurate fit to the local linear toroidal response function, which is derived in this section.

We begin by transforming the linearized gyrokinetic equation to (E, μ) variables, so $F = F(\mathbf{R}, E, \mu)$, where $E = v_\parallel^2/2 + \mu B$. Then breaking F into adiabatic and nonadiabatic pieces, $F = g - F_0 J_0 \, e\Phi/T_0$, the equation for the nonadiabatic piece is found to be:

$$g = F_0 \frac{\omega - \omega_*^T}{\omega - k_\parallel v_\parallel - \omega_{dv}} J_0 \frac{e\Phi}{T_0}, \tag{49}$$

where $\omega_{dv} = \omega_d(v_\parallel^2 + \mu B)/v_t^2$ and $\omega_*^T = \omega_*[1 + \eta(v_\parallel^2/2v_t^2 + \mu B/v_t^2 - 3/2)]$. In the local approximation, we treat ω_d, ω_*, and $k_\parallel$ as constants, using $\omega_d = -k_\theta \rho v_t/R$ and $\omega_* = -k_\theta \rho v_t/L_n$, so $\omega_d/\omega_* = L_n/R \equiv \epsilon_n$. The total distribution function in guiding center coordinates, $f = f(\mathbf{R}, E, \mu)$ is:

$$f(\mathbf{R}) = F + \tilde{f} = F(\mathbf{R}) - \frac{e\Phi(\mathbf{x})}{T_0} F_0 + F_0 J_0 \frac{e\Phi(\mathbf{R})}{T_0}. \tag{50}$$

where F is gyrophase independent, and $\tilde{f}$ is the gyrophase dependent part. The first piece of $\tilde{f}$ is in real space, $\mathbf{x}$. To obtain the real space ion density (not the density of gyrocenters), only the parts in guiding center space need to be gyroaveraged (acted on by J_0):

$$\begin{aligned} n(\mathbf{x}) = \int d^3v f(\mathbf{x}) &= \int d^3v \left[J_0 F(\mathbf{R}) - \frac{e\Phi(\mathbf{x})}{T_0} F_0 + F_0 J_0^2 \frac{e\Phi(\mathbf{R})}{T_0} \right] \\ &= -n_0 \frac{e\Phi}{T_0} + \int d^3v J_0 g, \end{aligned} \tag{51}$$

since the $J_0 F$ and $F_0 J_0^2\, e\Phi/T_0$ pieces combine to give $J_0 g$. Inserting the solution for g, Eq. (49), the ion density response function is:

$$R_i = \frac{n}{-n_0 e\Phi/T_0} = 1 - \frac{1}{n_0}\int d^3v F_0 \frac{\omega - \omega_*^T}{\omega - k_\parallel v_\parallel - \omega_{dv}} J_0^2(k_\perp v_\perp/\Omega), \tag{52}$$

which is the usual linear form. Trapped particle effects appear in the variation of $v_\parallel$ along a particle's orbit. We will neglect trapped particle effects in this section, and treat $v_\parallel$ as a constant.

For $\mathrm{Im}(\omega/\omega_d) > 0$, the resonant denominator can be written:

$$\frac{1}{\omega - k_\parallel v_\parallel - \omega_{dv}} = -\frac{i}{\omega_d}\int_0^\infty d\tau\, e^{i\tau(\omega - k_\parallel v_\parallel - \omega_{dv})/\omega_d}, \tag{53}$$

and now the $v_\parallel$ and $v_\perp$ integrals can be evaluated. Normalizing ω and $k_\parallel v_t$ to the toroidal drift frequency by introducing $x = \omega/\omega_d$ and $z_\parallel = k_\parallel v_t/\omega_d$, and using a Maxwellian F_0, Eq. (12), the response function becomes:

$$R_i = 1 + \frac{i}{\sqrt{2\pi}}\int_0^\infty d\tau \int_0^\infty dv_\perp v_\perp \int_{-\infty}^\infty dv_\parallel \left\{ x - \frac{1}{\epsilon_n}\left[1 + \eta(\frac{v_\parallel^2 + v_\perp^2}{2v_t^2} - \frac{3}{2})\right]\right\}$$
$$\times e^{i\tau[x - z_\parallel v_\parallel/v_t - v_\parallel^2/v_t^2 - v_\perp^2/2v_t^2]} e^{-(v_\parallel^2 + v_\perp^2)/2v_t^2} J_0^2(k_\perp v_\perp/\Omega)$$

The $v_\perp$ integrals are:

$$\int_0^\infty dv_\perp v_\perp e^{-(1+i\tau)v_\perp^2/2v_t^2} J_0^2(\sqrt{b}v_\perp/v_t) = v_t^2 \frac{e^{-b/(1+i\tau)}}{1+i\tau} I_0\left(\frac{b}{1+i\tau}\right), \tag{54}$$

and

$$\int_0^\infty dv_\perp v_\perp^3 e^{-(1+i\tau)v_\perp^2/2v_t^2} J_0^2(\sqrt{b}v_\perp/v_t) = \tag{55}$$
$$2v_t^2 \frac{e^{-b/(1+i\tau)}}{(1+i\tau)^2} I_0\left(\frac{b}{1+i\tau}\right)\left[1 - \frac{b}{1+i\tau} + \frac{b}{1+i\tau}\frac{I_1(b/1+i\tau)}{I_0(b/1+i\tau)}\right],$$

where I_0 and I_1 are modified Bessel functions. The $v_\perp$ dependence in the resonant denominator was neglected in the numerical evaluation of the $v_\perp$ integrals of J_0 in Ref. 8 (although it was retained everywhere else), and thus I_0 and I_1 had real arguments, instead of the complex arguments in the expressions above. This produces differences in the local dispersion relations at large b. The

response function in Ref. 27 correctly retains the $v_\perp$ dependence of the resonant denominator while integrating over $v_\perp$. The local kinetic response function described here, and the local kinetic eigenvalues calculated using this response function in Section IX, were carefully checked against the results of Ref. 27.

The $v_\parallel$ integrals are:

$$\int_0^\infty dv_\parallel e^{-(1+2i\tau)v_\parallel^2/2v_t^2 - i\tau z_\parallel v_\parallel/v_t} = \sqrt{2\pi} v_t \frac{e^{-\tau^2 z_\parallel^2/2(1+2i\tau)}}{\sqrt{1+2i\tau}}, \tag{56}$$

and

$$\int_0^\infty dv_\parallel v_\parallel^2 e^{-(1+2i\tau)v_\parallel^2/2v_t^2 - i\tau z_\parallel v_\parallel/v_t} = \sqrt{2\pi} v_t^3 \frac{e^{-\tau^2 z_\parallel^2/2(1+2i\tau)}}{(1+2i\tau)^{5/2}}(1+2i\tau-\tau^2 z_\parallel^2). \tag{57}$$

Putting it all together:

$$R_i = 1 + i\int_0^\infty d\tau\, e^{i\tau x} e^{-\tau^2 z_\parallel^2/2(1+2i\tau)} e^{-b/(1+i\tau)} I_0\left(\frac{b}{1+i\tau}\right)\left\{\frac{x-(1-\frac{3}{2}\eta_i)/\epsilon_n}{(1+i\tau)\sqrt{1+2i\tau}}\right. \tag{58}$$

$$\left. -\frac{\eta_i}{\epsilon_n}\left[\frac{1-\frac{b}{1+i\tau}+\frac{b}{1+i\tau}I_1(\frac{b}{1+i\tau})/I_0\left(\frac{b}{1+i\tau}\right)}{(1+i\tau)^2\sqrt{1+2i\tau}}\right] - \frac{\eta_i}{\epsilon_n}\left[\frac{1+2i\tau-\tau^2 z_\parallel^2}{2(1+i\tau)(1+2i\tau)^{5/2}}\right]\right\},$$

Thus, the local toroidal response function is a rather complicated function, $R_i = R_i(x,\, z_\parallel,\, b,\, \epsilon_n,\, \eta)$. We wish to find closure approximations so the response derived from the fluid equations will closely match this response function. In the form of a one dimensional integral as in Eq. (58), the response function is easy to evaluate numerically, which we will be forced to do to find the optimal closure coefficients and to solve the local dispersion relation. The response function can be factored into three pieces, the first independent of ω_*, the second proportional to $1/\epsilon_n$, and the third proportional to η/ϵ_n. Since we will be interested in matching this kinetic response for all η and ϵ_n, we need to fit each of these pieces independently:

$$R_i = R_0 + R_1/\epsilon_n + R_2\eta/\epsilon_n, \tag{59}$$

where R_0, R_1, and R_2 are independent of η and ϵ_n:

$$R_0 = 1 + i\int_0^\infty d\tau\, e^{i\tau x} e^{-\tau^2 z_\parallel^2/2(1+2i\tau)} e^{-b/(1+i\tau)} I_0\left(\frac{b}{1+i\tau}\right)\left\{\frac{x}{(1+i\tau)\sqrt{1+2i\tau}}\right\}, \tag{60}$$

$$R_1 = -i\int_0^\infty d\tau\, e^{i\tau x} e^{-\tau^2 z_\parallel^2/2(1+2i\tau)} e^{-b/(1+i\tau)} I_0\left(\frac{b}{1+i\tau}\right)\left\{\frac{1}{(1+i\tau)\sqrt{1+2i\tau}}\right\} \tag{61}$$

$$R_2 = i\int_0^\infty d\tau\, e^{i\tau x} e^{-\tau^2 z_\parallel^2/2(1+2i\tau)} e^{-b/(1+i\tau)} I_0\left(\frac{b}{1+i\tau}\right)\left\{\frac{3/2}{(1+i\tau)\sqrt{1+2i\tau}}\right. \tag{62}$$

$$\left. -\frac{1-\frac{b}{1+i\tau}+\frac{b}{1+i\tau}I_1(\frac{b}{1+i\tau})/I_0(\frac{b}{1+i\tau})}{(1+i\tau)^2\sqrt{1+2i\tau}} - \frac{1+2i\tau-\tau^2 z_\parallel^2}{2(1+i\tau)(1+2i\tau)^{5/2}}\right\},$$

The response function of the fluid equations will also naturally factor into these three parts. In the purely toroidal limit ($k_\parallel = 0$), neglecting FLR ($b = 0$), these expressions simplify considerably, and can be written in terms of the usual plasma dispersion function:[28]

$$R_0 = 1 - \frac{x}{2} Z^2\left(\sqrt{\frac{x}{2}}\right) \tag{63}$$

$$R_1 = \frac{1}{2} Z^2\left(\sqrt{\frac{x}{2}}\right) \tag{64}$$

$$R_2 = \left(\frac{x}{2} - \frac{1}{2}\right) Z^2\left(\sqrt{\frac{x}{2}}\right) + \sqrt{\frac{x}{2}} Z\left(\sqrt{\frac{x}{2}}\right) \tag{65}$$

The resonant denominator in Eq. (52), $\omega - k_\parallel v_\parallel - \omega_d(v_\parallel^2 + v_\perp^2/2)/v_t^2 = 0$, by completing the square, can be written:

$$\frac{\omega}{\omega_d} + \frac{k_\parallel^2 v_t^2}{4\omega_d^2} = \left(\frac{k_\parallel v_t}{2\omega_d} + \frac{v_\parallel}{v_t}\right)^2 + \frac{v_\perp^2}{2v_t^2}. \tag{66}$$

The left hand side of Eq. (66) is negative, but the right hand side is positive for all v. Thus along the real ω axis, no particles are in resonance for $\omega < -k_\parallel^2 v_t^2/4\omega_d$, and R_i is purely real, as shown in Figs. 1 and 2. As $k_\parallel \to \infty$, this cutoff frequency moves to $-\infty$, and R_i approaches the slab limit response function. A useful discussion of this transition from the toroidal resonance to the slab resonance and the resulting change in the local kinetic ITG threshold is given in Ref. 29.

We will also use the kinetic response function of other moments (not just density), which can be written in the following compact form in the $b = 0$ limit:

$$M_{j,k} = \int d^3v f v_\parallel^j (v_\perp^2/2)^k = -n_0 v_t^{2k+j} \frac{e\Phi}{T_0} \tilde{M}_{j,k} \tag{67}$$

$$\tilde{M}_{j,k} = \tilde{M}_{j,k}^{(0)} + \tilde{M}_{j,k}^{(1)}/\epsilon_n + \tilde{M}_{j,k}^{(2)}\eta/\epsilon_n \tag{68}$$

$$\tilde{M}_{j,k} = \frac{2^{j/2}}{\sqrt{\pi}} \frac{1+(-1)^j}{2} \Gamma(k+1)\Gamma(\frac{j+1}{2}) + i2^{-j/2} \int d\tau\, e^{i\tau x} \times \tag{69}$$

$$\left\{ \left[x - \frac{1}{\epsilon_n} + \frac{3}{2}\frac{\eta}{\epsilon_n} - \frac{\eta}{\epsilon_n}\frac{k+1}{1+i\tau} \right] \tilde{K}_j - \frac{\eta}{\epsilon_n} \tilde{K}_{j+2} \right\} \frac{\Gamma(k+1) e^{-\tau^2 z_\parallel^2/2(1+2i\tau)}}{(1+i\tau)^{k+1}(1+2i\tau)^{j+1/2}}$$

$$\tilde{K}_j = \frac{2^{j/2}(1+2i\tau)^{j+1/2}}{\sqrt{2\pi} v_t^{j+1}} e^{\tau^2 z_\parallel^2/2(1+2i\tau)} \int_{-\infty}^{\infty} dv_\parallel v_\parallel^j e^{-(1+2i\tau)v_\parallel^2/2v_t^2 - i\tau z_\parallel v_\parallel/v_t} \tag{70}$$

For the lowest few j's, we have:

$$\begin{aligned}
\tilde{K}_0 &= 1, \\
\tilde{K}_1 &= -i\tau z_\parallel, \\
\tilde{K}_2 &= 2(1+2i\tau) - \tau^2 z_\parallel^2, \\
\tilde{K}_3 &= \tau z_\parallel [-6i(1+2i\tau) + i\tau^2 z_\parallel^2)], \\
\tilde{K}_4 &= 12(1+2i\tau)^2 - 12\tau^2 z_\parallel^2 (1+2i\tau) + \tau^4 z_\parallel^4.
\end{aligned}$$

The odd $\tilde{K}_j$'s are proportional to odd powers of $z_\parallel$ (or $k_\parallel$), while the even $\tilde{K}_j$'s are proportional to even powers of $z_\parallel$. This will guide our choice of closure approximations in the next section.

VI. General Closure

There are three places in the moment equations Eqs. (38)-(41) where closure approximations are needed, in addition to the FLR closures in Section IV): in the parallel free streaming terms $\nabla_\parallel r_{\parallel,\parallel}$ and $\nabla_\parallel r_{\parallel,\perp}$; in the toroidal drift terms $\omega_d(r_{\parallel,\parallel} + r_{\parallel,\perp})$, $\omega_d(r_{\parallel,\perp} + r_{\perp,\perp})$, $\omega_d(s_{\parallel,\parallel} + s_{\parallel,\perp})$, and $\omega_d(s_{\parallel,\perp} + s_{\perp,\perp})$; and in the mirroring terms $r_{\parallel,\parallel}\nabla_\parallel \ln B$, $r_{\parallel,\perp}\nabla_\parallel \ln B$, and $r_{\perp,\perp}\nabla_\parallel \ln B$. For each, we make closure approximations designed to model the physical processes these terms represent. Because our final closure scheme is rather complicated, we begin by considering simple models of phase mixing arising from parallel free streaming and toroidal drifts independently, to justify the functional forms of our closures. Then, we consider both resonances together, and find closure coefficients which ensure that the fluid response function closely matches the kinetic response function for all $k_\parallel$ and ω_d. Because of the branch cut discontinuity at $\omega_d = 0$ in the toroidal limit

response function, we will not be able to use analytic methods to find the closure coefficients, as was done in Refs. 5 and 9. We will therefore find the toroidal closure coefficients by numerically minimizing the difference between the fluid and kinetic responses.

The velocity dependence in the $k_\parallel v_\parallel$ parallel term introduces parallel phase mixing, leading to linear Landau damping. Consider a simple 1D kinetic equation with no $\mathbf{E}$ field:

$$\frac{\partial f}{\partial t} + v_\parallel \frac{\partial f}{\partial z} = 0. \tag{71}$$

The solution is simply $f(z, v_\parallel, t) = f(z - v_\parallel t, v_\parallel, t = 0)$. If we start with a Maxwellian perturbation in f,

$$f_0 = e^{ik_\parallel z} f_M = e^{ik_\parallel z} \frac{n_0}{\sqrt{2\pi v_t^2}} e^{-v_\parallel^2/2v_t^2}, \tag{72}$$

free streaming will cause moments of f to phase mix away. For example, the density is:

$$n = \int d^3v\, f = \frac{n_0}{\sqrt{2\pi v_t^2}} \int dv_\parallel\, e^{ik_\parallel (z - v_\parallel t)} e^{-v_\parallel^2/2v_t^2} = n_0 e^{ik_\parallel z} e^{-k_\parallel^2 v_t^2 t^2/2}. \tag{73}$$

To model this process, we need to introduce damping proportional to $|k_\parallel| v_t$ into our fluid equations. Thus, for the parallel closures, we choose:[5,9]

$$r_{\parallel,\parallel} = 3(2p_\parallel - n) + \beta_\parallel T_\parallel - i\sqrt{2} D_\parallel \frac{|k_\parallel|}{k_\parallel} q_\parallel, \tag{74}$$

$$r_{\parallel,\perp} = p_\parallel + p_\perp - n - i\sqrt{2} D_\perp \frac{|k_\parallel|}{k_\parallel} q_\perp, \tag{75}$$

where $\beta_\parallel = (32 - 9\pi)/(3\pi - 8)$, $D_\parallel = 2\sqrt{\pi}/(3\pi - 8)$, and $D_\perp = \sqrt{\pi}/2$. With this closure, the fluid equations reproduce the linear kinetic behavior quite well in the slab limit, as shown in Refs. 5 and 9.

Similarly, the velocity dependence of the ∇B and curvature drifts introduces phase mixing. In this case the damping rate is different, since the toroidal drifts depend on $v_\parallel^2$ and $v_\perp^2/2$. Now consider only the phase mixing due to the toroidal drifts:

$$\frac{\partial f}{\partial t} + v_d \frac{\partial f}{\partial y} = 0, \tag{76}$$

$$v_d = v_{d0}\frac{v_\parallel^2 + v_\perp^2/2}{v_t^2}, \qquad\qquad v_{d0} = \frac{\rho v_t}{R}.$$

The solution is $f(y, v_\parallel, v_\perp, t) = f(y - v_d t, v_\parallel, v_\perp, t = 0)$. Starting with a Maxwellian perturbation in f,

$$f_0 = e^{ik_y y} f_M = e^{ik_y y}\frac{n_0}{(2\pi v_t^2)^{3/2}} e^{-(v_\parallel^2 + v_\perp^2)/2v_t^2}, \tag{77}$$

free streaming will again cause moments of f to phase mix away. For example, the density is:

$$\begin{aligned} n = \int d^3v\, f &= \frac{n_0}{(2\pi v_t^2)^{3/2}} 2\pi \int dv_\parallel dv_\perp v_\perp e^{ik_y y - v_{d0}[v_\parallel^2/v_t^2 - v_\perp^2/2v_t^2)t]} e^{-(v_\parallel^2 + v_\perp^2)/2v_t^2} \\ &= \frac{n_0 e^{ik_y y}}{\sqrt{1 + 2ik_y v_{d0} t}(1 + ik_y v_{d0} t)}. \end{aligned} \tag{78}$$

To capture this toroidal phase mixing, damping proportional to $|k_y| v_{d0} = |\omega_d|$ must be introduced into the fluid equations, but with complex closure coefficients to get the phase shift in Eq. (78).

The toroidal closure terms enter in the combinations $r_{\parallel,\parallel} + r_{\parallel,\perp}$, $r_{\parallel,\perp} + r_{\perp,\perp}$, $s_{\parallel,\parallel} + s_{\parallel,\perp}$, and $s_{\parallel,\perp} + s_{\perp,\perp}$. Expanding the general moment response functions Eq. (69) for small $k_\parallel$, all the odd j moments have leading order corrections of $\mathcal{O}(k_\parallel)$, while the even j moments have leading order corrections of $\mathcal{O}(k_\parallel^2)$. Thus in our closure approximations for the toroidal terms, we close the even moments $r_{\parallel,\parallel} + r_{\parallel,\perp}$ and $r_{\parallel,\perp} + r_{\perp,\perp}$ in terms of the lower even moments (n, $p_\parallel$, and $p_\perp$), and the odd moments $s_{\parallel,\parallel} + s_{\parallel,\perp}$ and $s_{\parallel,\perp} + s_{\perp,\perp}$ in terms of the lower odd moments ($u_\parallel$, $q_\parallel$, and $q_\perp$), to preserve this small $k_\parallel$ behavior. At large $k_\parallel$ (the slab limit) the response function is primarily determined by the parallel closures, and the toroidal closure approximations are subdominant. In addition, we break the r and s closures into dissipative and Maxwellian pieces (the terms that would arise if F was exactly Maxwellian). The Maxwellian parts are $r_{\parallel,\parallel} = 3p_\parallel^2/n$, $r_{\parallel,\perp} = p_\parallel p_\perp/n$, $r_{\perp,\perp} = 2p_\perp^2/n$, and $s_{\parallel,\parallel} = s_{\parallel,\perp} = s_{\perp,\perp} = 0$. Linearizing and normalizing, these become $r_{\parallel,\parallel} = 6p_\parallel - 3n$, $r_{\parallel,\perp} = p_\parallel + p_\perp - n$, and $r_{\perp,\perp} = 4p_\perp - 2n$. Guided by the discussion above, we choose dissipative pieces proportional to $|\omega_d|/\omega_d$. Thus in the toroidal terms, combining the Maxwellian and dissipative pieces, we choose:

$$r_{\parallel,\parallel} + r_{\parallel,\perp} \;=\; 7p_\parallel + p_\perp - 4n - 2i\frac{|\omega_d|}{\omega_d}(\nu_1 T_\parallel + \nu_2 T_\perp) \tag{79}$$

$$r_{\parallel,\perp} + r_{\perp,\perp} = p_\parallel + 5p_\perp - 3n - 2i\frac{|\omega_d|}{\omega_d}\left(\nu_3 T_\parallel + \nu_4 T_\perp\right) \tag{80}$$

$$s_{\parallel,\parallel} + s_{\parallel,\perp} = -i\frac{|\omega_d|}{\omega_d}\left(\nu_5 u_\parallel + \nu_6 q_\parallel + \nu_7 q_\perp\right) \tag{81}$$

$$s_{\parallel,\perp} + s_{\perp,\perp} = -i\frac{|\omega_d|}{\omega_d}\left(\nu_8 u_\parallel + \nu_9 q_\parallel + \nu_{10} q_\perp\right) \tag{82}$$

Each closure coefficient has both a dissipative and non-dissipative piece, $\nu = \nu_r + i\nu_i|\omega_d|/\omega_d$. This choice is motivated by Ref. 8. Making the dissipative parts of the r closures only depend on $T_\parallel$ and $T_\perp$ ensures that the fluid response will match the kinetic response at $\omega/\omega_d = 0$ in the $k_\parallel = 0$ limit.

The toroidal closure coefficients $\nu_1 - \nu_{10}$ in Eqs. (79-80) are chosen so the response function of the fluid equations closely approximates kinetic response function, Eq. (58). In the local limit with $b = 0$ and $\nabla_\parallel B = 0$, and inserting the closure approximations above, the fluid equations Eqs. (36-41) can be written in matrix form, using $g \equiv \omega_d/\omega = 1/x$ and $k = k_\parallel/\omega$, and assuming $\omega_d > 0$ to simplify notation:

$$M = \begin{bmatrix} 1 & -k & -g & -g & \cdots & 0 & 0 \\ 0 & 1-4g & -k & 0 & & -g & -g \\ g(4-2i\nu_1-2i\nu_2) & -3k & 1-g(7-2i\nu_1) & -g(1-2i\nu_2) & & -k & 0 \\ g(3-2i\nu_3-2i\nu_4) & -k & -g(1-2i\nu_3) & 1-g(5-2i\nu_4) & & 0 & -k \\ (3+\beta)k & -g(6-i\nu_5) & -(3+\beta)k & 0 & & 1+i\sqrt{2}D_\parallel k+g(3+i\nu_6) & g(3+i\nu_7) \\ k & -g(1-i\nu_8) & 0 & -k & & g(1+i\nu_9) & 1+i\sqrt{2}D_\perp k+g(1+i\nu_{10}) \end{bmatrix}$$

$$M\begin{bmatrix} n \\ u_\parallel \\ p_\parallel \\ p_\perp \\ q_\parallel \\ q_\perp \end{bmatrix} = \begin{bmatrix} 2 \\ k/g \\ 4 \\ 3 \\ 0 \\ 0 \end{bmatrix} g\Phi + \begin{bmatrix} -1 \\ 0 \\ -1 \\ -1 \\ 0 \\ 0 \end{bmatrix} \frac{g}{\epsilon_n}\Phi + \begin{bmatrix} 0 \\ 0 \\ -1 \\ -1 \\ 0 \\ 0 \end{bmatrix} \frac{g\eta}{\epsilon_n}\Phi \tag{83}$$

Thus, the response function of the fluid equations also naturally factors into the form Eq. (59). Because this set of equations is rather complicated, to determine the toroidal fluid response func-

tions we solve for n and $p_\perp$ by numerically row reducing the matrix M. In Ref. 8, the fluid and kinetic response functions were compared only in the $\omega_* = 0$ and $\eta = 0$ limit. In the slab limit, determining the closure coefficients in the $\omega_* = 0$ and $\eta = 0$ limit (R_0) also gave an equally good fit for the ω_* and η pieces (R_1 and R_2), but in the toroidal case this is not automatic. In addition, in Ref. 8 the toroidal closure coefficients were matched at $k_\parallel = 0$, and good agreement for $k_\parallel \neq 0$ is not guaranteed (although as $k_\parallel \to \infty$ the slab limit is recovered and the agreement will again be good). In fact, if the toroidal terms are closed in the purely toroidal limit ($k_\parallel = 0$), the toroidal closure terms in the odd moment equations drop out. This led to singular behavior of the response function for the closure in Ref. 8 at some non-zero $k_\parallel$, since the $\omega_d(q_\parallel + q_\perp)$ term in the parallel velocity equation was dropped. This was corrected in the addendum to that paper.

Therefore, special care must be taken find toroidal closure coefficients which simultaneously provide a good fit to the kinetic response function for all three parts of the response function, for all $k_\parallel$. Because both fluid and kinetic response functions are complicated with finite $k_\parallel$, we choose the closure coefficients numerically, by minimizing the difference between the kinetic and fluid response functions over a range of $k_\parallel$'s simultaneously, but in the $b = 0$ limit. We use an efficient multidimensional iterative minimization technique, Powell's method.[30] This process starts with arbitrary values of the coefficients $\nu_1 - \nu_{10}$, and numerically inverts the matrix M for these values of the coefficients for a specified range of x and $k_\parallel$. Then the difference between the fluid and kinetic response functions is calculated along the real x axis and the coefficients are adjusted. This process is repeated until the error between the kinetic and fluid is minimized, i.e., further small variations of the closure coefficients only make the fit worse. If R has no poles in the upper-half x plane, matching along the real axis guarantees that the fluid R will also match the kinetic R in the upper-half x plane. Since we are primarily interested in accurately modeling the growth rates of unstable modes, the errors in the lower half plane are probably not important, as long as we do have damped modes in the system. The best fit between the kinetic and fluid R's was found using 12 $k_\parallel$'s evenly spaced from $z_\parallel = 0$ to 4.2, over the range of x where the kinetic response function

is changing most rapidly, $-8 < x < 16$ at $z_\parallel = 0$ and $-14 < x < 22$ at $z_\parallel = 4.2$, with 100 grid points in x. To the error in the density response function, we also add $1/100$ the error between the kinetic and fluid $p_\perp$ responses, since n is most important for the local dispersion relation, but $p_\perp$ enters the linear dispersion relation from FLR effects. While an excellent fit to n is obtained, it is difficult to simultaneously match the $p_\perp$ response for intermediate $k_\parallel$'s. We find that the best fit is given by $\nu_1 = (2.019, -1.620)$, $\nu_2 = (0.433, 1.018)$, $\nu_3 = (-0.256, 1.487)$, $\nu_4 = (-0.070, -1.382)$, $\nu_5 = (-8.927, 12.649)$, $\nu_6 = (8.094, 12.638)$, $\nu_7 = (13.720, 5.139)$, $\nu_8 = (3.368, -8.110)$, $\nu_9 = (1.974, -1.984)$, and $\nu_{10} = (8.269, 2.060)$. This set of the closure coefficients results in a fluid response function which differs from the kinetic response function by an RMS average of 0.044 (in the real and imaginary parts) over the range specified above. Outside this range, the difference is even smaller, since for large x the response is fluid-like and the fluid equations automatically do quite well, and for large $k_\parallel$ (the slab limit), the response is slab-like and the agreement is quite good, as shown in Refs. 5 and 9. These are an improvement over the closure coefficients in Ref. 11. The fit between the kinetic and fluid response functions is excellent, as shown in Figs. 1 and 2. The fluid equations give a rational approximation to the kinetic response function, and cannot capture the branch cut at $\omega/\omega_d = -k_\parallel^2 v_t^2/4\omega_d^2$ exactly (see Eq. (66)), but this set of closure approximations provides a reasonable fit to this sharp transition.

Finally, we have to close the mirroring terms, introduced by the $\mu\hat{\mathbf{b}}\cdot\nabla B$ terms in the gyrokinetic equation. These terms incorporate trapped particle effects, reproducing the CGL[31] pressure balance equation. They are also important to model the damping of poloidal flows by magnetic pumping. Since these terms introduce no new dissipative processes, we take Maxwellian closures:

$$r_{\parallel,\parallel} = 6p_\parallel - 3n, \tag{84}$$

$$r_{\parallel,\perp} = p_\parallel + p_\perp - n, \tag{85}$$

$$r_{\perp,\perp} = 4p_\perp - 2n. \tag{86}$$

This may not be the ultimate set of closure approximations, however, the resulting fluid equa-

tions provide a very accurate model of the physics underlying ion dynamics in toroidal plasmas. While it is straightforward to calculate the error between the kinetic and fluid response functions, it is more difficult to quantify the accuracy of the fluid eigenfrequencies, or roots of the dispersion relation. As shown in Sec. IX, this set of closures provides excellent agreement with linear kinetic calculations, as long as one is not too close to marginal stability, where the small errors in the response function can give rise to weakly unstable modes. We have obtained another set of closure coefficients designed give a more accurate threshold, by minimizing the error in the response function and threshold simultaneously. These coefficients are: $\nu_1 = (0.848, -0.118)$, $\nu_2 = (-1.239, 2.064)$, $\nu_3 = (0.103, -0.517)$, $\nu_4 = (0.960, -1.906)$, $\nu_5 = (-11.626, 3.185)$, $\nu_6 = (-2.872, 11.679)$, $\nu_7 = (-3.156, 9.878)$, $\nu_8 = (4.494, 1.225)$, $\nu_9 = (3.260, 4.625)$, and $\nu_{10} = (5.888, 10.459)$. Unfortunately, while improving the threshold behavior, these coefficients are less accurate than the above set away from threshold. More complicated closure approximations could certainly be found, or the set of equations used here could be extended to higher moments, but the relative simplicity of the closures used here afford a tractable and sufficiently accurate model for most applications.

VII. Final Equations

We arrive at the six moment toroidal gyrofluid equations by inserting the closures discussed in the previous section into the moment equations, Eqs. (36)-(41), with the nonlinear terms given by Eqs. (42)-(47). Specifically, we use the parallel phase mixing closures in Eqs. (74)-(75), the toroidal phase mixing closures in Eqs. (79)-(82), and Maxwellian closures for the mirroring terms, Eqs. (84)-(86). In addition, we add the collision terms obtained by integrating Eq. (6) over velocity space. We will also refer to this set of equations as the "4+2" model, since it evolves 4 parallel moments and 2 perpendicular moments.

$$\begin{aligned} \frac{dn}{dt} &+ [\frac{1}{2}\hat{\nabla}_\perp^2 \mathbf{v}_\Psi] \cdot \nabla T_\perp + B\nabla_\parallel \frac{u_\parallel}{B} - \left(1 + \frac{\eta_\perp}{2}\hat{\nabla}_\perp^2\right) i\omega_* \Psi \\ &+ \left(2 + \frac{1}{2}\hat{\nabla}_\perp^2\right) i\omega_d \Psi + i\omega_d (p_\parallel + p_\perp) = 0, \end{aligned} \tag{87}$$

$$\frac{du_\parallel}{dt} + [\frac{1}{2}\hat{\nabla}_\perp^2 \mathbf{v}_\Psi] \cdot \nabla q_\perp + B\nabla_\parallel \frac{p_\parallel}{B} + \nabla_\parallel \Psi + \left(p_\perp + \frac{1}{2}\hat{\nabla}_\perp^2 \Psi\right) \nabla_\parallel \ln B \tag{88}$$
$$+ i\omega_d(q_\parallel + q_\perp + 4u_\parallel) = 0,$$

$$\frac{dp_\parallel}{dt} + [\frac{1}{2}\hat{\nabla}_\perp^2 \mathbf{v}_\Psi] \cdot \nabla T_\perp + B\nabla_\parallel \frac{q_\parallel + 3u_\parallel}{B} + 2(q_\perp + u_\parallel)\nabla_\parallel \ln B \tag{89}$$
$$- \left(1 + \eta_\parallel + \frac{\eta_\perp}{2}\hat{\nabla}_\perp^2\right) i\omega_* \Psi + \left(4 + \frac{1}{2}\hat{\nabla}_\perp^2\right) i\omega_d \Psi + i\omega_d(7p_\parallel + p_\perp - 4n)$$
$$+ 2|\omega_d|(\nu_1 T_\parallel + \nu_2 T_\perp) = -\frac{2}{3}\nu_{ii}(p_\parallel - p_\perp),$$

$$\frac{dp_\perp}{dt} + [\frac{1}{2}\hat{\nabla}_\perp^2 \mathbf{v}_\Psi] \cdot \nabla p_\perp + [\hat{\hat{\nabla}}_\perp^2 \mathbf{v}_\Psi] \cdot \nabla T_\perp + B^2 \nabla_\parallel \frac{q_\perp + u_\parallel}{B^2} \tag{90}$$
$$- \left[1 + \frac{1}{2}\hat{\nabla}_\perp^2 + \eta_\perp\left(1 + \frac{1}{2}\hat{\nabla}_\perp^2 + \hat{\hat{\nabla}}_\perp^2\right)\right] i\omega_* \Psi + \left(3 + \frac{3}{2}\hat{\nabla}_\perp^2 + \hat{\hat{\nabla}}_\perp^2\right) i\omega_d \Psi$$
$$+ i\omega_d(5p_\perp + p_\parallel - 3n) + 2|\omega_d|(\nu_3 T_\parallel + \nu_4 T_\perp) = \frac{1}{3}\nu_{ii}(p_\parallel - p_\perp),$$

$$\frac{dq_\parallel}{dt} + (3 + \beta_\parallel)\nabla_\parallel T_\parallel + \sqrt{2}D_\parallel |k_\parallel| q_\parallel + i\omega_d(-3q_\parallel - 3q_\perp + 6u_\parallel) \tag{91}$$
$$+ |\omega_d|(\nu_5 u_\parallel + \nu_6 q_\parallel + \nu_7 q_\perp) = -\nu_{ii} q_\parallel,$$

$$\frac{dq_\perp}{dt} + [\frac{1}{2}\hat{\nabla}_\perp^2 \mathbf{v}_\Psi] \cdot \nabla u_\parallel + [\hat{\hat{\nabla}}_\perp^2 \mathbf{v}_\Psi] \cdot \nabla q_\perp + \nabla_\parallel \left(T_\perp + \frac{1}{2}\hat{\nabla}_\perp^2 \Psi\right) \tag{92}$$
$$+ \sqrt{2}D_\perp |k_\parallel| q_\perp + \left(p_\perp - p_\parallel + \hat{\hat{\nabla}}_\perp^2 \Psi - \frac{1}{2}\hat{\nabla}_\perp^2 \Psi\right) \nabla_\parallel \ln B$$
$$+ i\omega_d(-q_\parallel - q_\perp + u_\parallel) + |\omega_d|(\nu_8 u_\parallel + \nu_9 q_\parallel + \nu_{10} q_\perp) = -\nu_{ii} q_\perp.$$

The main $\mathbf{E} \times \mathbf{B}$ nonlinearities have been absorbed in the total time derivative $d/dt = \partial/\partial t + \mathbf{v}_\Psi \cdot \nabla$. In the slab limit ($\omega_d = \nabla_\parallel \ln B = 0$) these equations reduce to Eqs. (56)-(61) of Ref. 9. The quasineutrality constraint is:

$$n_e = \frac{n}{1 + b/2} - \frac{bT_\perp}{2(1 + b/2)^2} + (\Gamma_0 - 1)\Phi. \tag{93}$$

When the electrons are assumed to be adiabatic,

$$n_e = \tau(\Phi - \langle\Phi\rangle), \tag{94}$$

where $\tau = T_{i0}/T_{e0}$ and $\langle\Phi\rangle$ is a flux surface average.

This constitutes a fairly complicated set of fluid equations compared to those usually used in plasma physics. A somewhat simpler four moment model is described below, and it is worth jus-

tifying the complication of the six moment model. In principle, the six moment model is more appealing because as more moments are retained, more details of the distribution function are accurately described. On more pragmatic grounds, the six moment model provides a significantly improved fit to the kinetic response function, and is necessary for quantitative accuracy in linear growth rates and mode structures. The six moment model is also required to capture the destabilization from trapped ion effects, which become important in the long wavelength regime. Finally, six moments may be required to obtain accurate damping rates of poloidal flows from magnetic pumping. Magnetic pumping arises from parallel flow damping, and since no closure approximations appear in Eq. (88), the $u_\parallel$ equation is an exact moment of the gyrokinetic equation to $\mathcal{O}(b)$. This is not the case for the simpler four moment model discussed below. Magnetic pumping rates from this six moment model are calculated in Ref. 7.

A variation of these equations was used in Ref. 11 where $|k_\parallel|q_\parallel$ in Eq. (91) was replaced by $B|k_\parallel|(q_\parallel/B)$ and where $|k_\parallel|q_\perp$ in Eq. (92) was replaced by $B^2|k_\parallel|(q_\perp/B^2)$, i.e. $|k_\parallel|$ acted on $q_\perp/B^2$, not just $q_\perp$. However, it was found that this leads to a weakly growing mode even in the $\omega_d = \omega_* = \eta = 0$ limit which should be stable (a bumpy cylinder limit). Switching to the present form of the parallel closures removed this spurious instability.

VIII. Four Moment Model

We present here a simpler and slightly less accurate gyrofluid model which only evolves four moments: n, $u_\parallel$, $p_\parallel$, and $p_\perp$. We will also refer to this set of equations as the "3+1" model, since it evolves three parallel moments and one perpendicular moment. In this case, since we are not evolving $q_\parallel$ and $q_\perp$, instead of closing the toroidal s terms with Eqs. (81) and (82), we need to close the $\omega_d(q_\parallel + q_\perp)$ term in the parallel velocity equation:

$$q_\parallel + q_\perp = -2i\frac{|\omega_d|}{\omega_d}\nu_5 u_\parallel. \tag{95}$$

We still use the toroidal r closures in Eqs. (79) and (80), but with new closure coefficients. In addition, we use the parallel closures of Ref. 5 and 9, extended to include collisions as well as collisionless phase mixing:

$$q_\parallel = -\frac{3+\beta_\parallel}{\sqrt{2}D_\parallel|k_\parallel|+\nu_{ii}} ik_\parallel T_\parallel \tag{96}$$

$$q_\perp = -\frac{1}{\sqrt{2}D_\perp|k_\parallel|+\nu_{ii}} ik_\parallel \left(T_\perp + \frac{1}{2}\hat{\nabla}_\perp^2\Psi\right) \tag{97}$$

These are essentially the high $k_\parallel$ and/or high ν_{ii} limits of Eqs. (91) and (92), keeping only the slab terms.

We again use the method described in Section VI to minimize the error between the fluid and kinetic local response functions to determine the toroidal closure coefficients $\nu_1 - \nu_5$. The best fit is $\nu_1 = (1.232, 0.437)$, $\nu_2 = (-0.912, 0.362)$, $\nu_3 = (-1.164, 0.294)$, $\nu_4 = (0.478, -1.926)$, and $\nu_5 = (0.515, -0.958)$.

Inserting these q closures into Eqs. (36)-(39), using the nonlinear FLR terms in Eqs. (42)-(45) without the $q_\perp$ part of Eq. (43), and dropping the $q_\parallel$ and $q_\perp$ mirroring terms ($q_\parallel = q_\perp = 0$ for a Maxwellian), the dynamical equations are:

$$\begin{aligned}
\frac{dn}{dt} &+ [\frac{1}{2}\hat{\nabla}_\perp^2\mathbf{v}_\Psi]\cdot\nabla T_\perp + B\nabla_\parallel\frac{u_\parallel}{B} - \left(1+\frac{\eta_\perp}{2}\hat{\nabla}_\perp^2\right) i\omega_*\Psi \qquad (98)\\
&+ \left(2+\frac{1}{2}\hat{\nabla}_\perp^2\right) i\omega_d\Psi + i\omega_d(p_\parallel + p_\perp) = 0,\\
\frac{du_\parallel}{dt} &+ B\nabla_\parallel\frac{p_\parallel}{B} + \nabla_\parallel\Psi + \left(p_\perp + \frac{1}{2}\hat{\nabla}_\perp^2\Psi\right)\nabla_\parallel \ln B + 4i\omega_d u_\parallel \qquad (99)\\
&+ 2|\omega_d|\nu_5 u_\parallel = 0,\\
\frac{dp_\parallel}{dt} &+ [\frac{1}{2}\hat{\nabla}_\perp^2\mathbf{v}_\Psi]\cdot\nabla T_\perp + \frac{(3+\beta_\parallel)k_\parallel^2 T_\parallel}{\sqrt{2}D_\parallel|k_\parallel|+\nu_{ii}} + 3\nabla_\parallel u_\parallel - u_\parallel\nabla_\parallel\ln B \qquad (100)\\
&- \left(1+\eta_\parallel+\frac{\eta_\perp}{2}\hat{\nabla}_\perp^2\right) i\omega_*\Psi + \left(4+\frac{1}{2}\hat{\nabla}_\perp^2\right) i\omega_d\Psi + i\omega_d(7p_\parallel + p_\perp - 4n)\\
&+ 2|\omega_d|(\nu_1 T_\parallel + \nu_2 T_\perp) = -\frac{2}{3}\nu_{ii}(p_\parallel - p_\perp),\\
\frac{dp_\perp}{dt} &+ [\frac{1}{2}\hat{\nabla}_\perp^2\mathbf{v}_\Psi]\cdot\nabla p_\perp + [\hat{\nabla}_\perp^2\mathbf{v}_\Psi]\cdot\nabla T_\perp + \frac{k_\parallel^2}{\sqrt{2}D_\perp|k_\parallel|+\nu_{ii}}(T_\perp + \frac{1}{2}\hat{\nabla}_\perp^2\Psi)
\end{aligned}$$

$$
\begin{aligned}
&+ \quad B^2\nabla_\parallel \frac{u_\parallel}{B^2} - \left[1 + \frac{1}{2}\hat{\nabla}_\perp^2 + \eta_\perp\left(1 + \frac{1}{2}\hat{\nabla}_\perp^2 + \hat{\hat{\nabla}}_\perp^{\,2}\right)\right] i\omega_* \Psi \qquad (101)\\
&+ \quad \left(3 + \frac{3}{2}\hat{\nabla}_\perp^2 + \hat{\hat{\nabla}}_\perp^{\,2}\right) i\omega_d \Psi + i\omega_d(5p_\perp + p_\parallel - 3n) + 2|\omega_d|(\nu_3 T_\parallel + \nu_4 T_\perp)\\
&= \quad \frac{1}{3}\nu_{ii}(p_\parallel - p_\perp).
\end{aligned}
$$

The quasineutrality constraint, Eq. (93), is unchanged for this model.

IX. Linear Benchmarks

In this section the accuracy of the toroidal gyrofluid equations is demonstrated by comparing with linear kinetic theory, using adiabatic electrons. We first test the toroidal gyrofluid equations against kinetic theory in the local limit, where $k_\parallel$ and ω_d are treated as constants. The eigenfrequencies are determined by finding roots of the local dispersion relation with adiabatic electrons, $R_i = -\tau$, where the kinetic R_i is calculated by numerically evaluating the integrals Eq. (59) and the fluid R_i is calculated by numerically row reducing the matrix equation in Eq. (83), with additional FLR terms on the right hand side if b is non-zero. In the local limit, we ignore the $\nabla_\parallel \ln B$ terms in the gyrofluid equations and ignore the modulation of $v_\parallel$ along a particle's orbit in the kinetic response.

Fig. 3 shows the kinetic and gyrofluid growth rates in the purely toroidal limit ($k_\parallel = 0$), with $b = 0$, for the parameters of Fig. 5a of Ref. 8, where $\tau = 1$, $\eta_i = 1$, 1.5, 2, and 3, varying ϵ_n. The four moment model in Section VIII reproduces the stable low ϵ_n regime better than the four moment model presented in Ref. 8 (which used different closure coefficients). The six moment equations provide much better agreement with kinetic theory, but are slightly off for low η_i, near marginal stability.

Fig. 4 shows a comparison in the local limit for $k_\parallel \neq 0$, the mixed toroidal/slab limit. We use the parameters of Fig. 3 of Ref. 32, where $\eta_i = 1.5, 2, 3$, $\epsilon_n = 0.2$, and we choose $k_\parallel L_n = L_n/qR = 0.1$, using the normal connection length for the mode width $L_\parallel \sim qR$, and $q = 2$. The linear growth rates from the six moment toroidal gyrofluid model and kinetic theory are shown vs. $k_\theta \rho_i$. The six

moment toroidal gyrofluid equations provide an accurate description of the full kinetic behavior. Both the growth rate and real frequency of the toroidal ITG mode vary roughly as $\gamma, \omega_r \propto k_\theta \rho_i$ at long wavelengths. As $k_\theta \rho_i$ decreases, $|\omega| = \sqrt{\gamma^2 + \omega_r^2}$ decreases, and the stabilizing effect of parallel Landau damping becomes more important. When $|\omega| \sim k_\parallel v_{ti}$, the mode is stabilized, producing the long wavelength cutoff at $k_\theta \rho_i \sim k_\parallel L_n \sim L_n/qR$. This local estimate suggests that the inverse q dependence of this long wavelength cutoff can introduce confinement degradation with increasing q, since the longest wavelengths cause the most transport.

Now we move on to nonlocal comparisons with kinetic theory using the ballooning representation in circular flux surface geometry, as in Ref. 32 and 33. In these nonlocal calculations, we find the eigenmode structure along the field line coordinate, θ, also called the "extended ballooning angle." The θ dependence of terms in the equations couples different $k_\parallel$'s; this coupling is ignored in the local approximation. For example, both ω_d and $k_\perp$ vary along the field line: the θ dependence of ω_d describes the effects of the good and bad curvature regions, and the θ dependence of $k_\perp$ comes from the fact that as one moves along the field line, the mode twists, and $k_\perp$ increases. For the comparison with Ref. 32, we neglect trapped particle effects by turning off the $\nabla_\parallel \ln B$ terms. In circular flux surface geometry, $B = B_0 R_0/R = B_0/(1+\epsilon \cos\theta)$, so setting $\epsilon = 0$ removes the $\nabla_\parallel \ln B$ mirroring terms. As in Ref. 32, we also neglect collisions and assume adiabatic electrons. All of the results compared in this section will only look at modes with $\theta_0 = 0$, i.e. those centered in the bad curvature region, since they are typically the most unstable and most linear calculations only focus on these modes. The growth rate spectrum for $\theta_0 \neq 0$ has important implications for the anisotropic fluctuation spectra seen in our nonlinear simulations and in experimental fluctuation measurements in tokamaks, as discussed in Ref. 7. Fig. 5 shows the eigenfunction from the fully kinetic integral calculation of Ref. 32 and from the 4+2 toroidal gyrofluid equations for the parameters in Fig. 2(c) of Ref. 32, $\eta_i = 3$, $\epsilon_n = 0.2$, $q = 2$, $\hat{s} = 1$, $k_\theta \rho_i = 0.53$, and $\tau = 1$. The "ballooning" mode structure along the field line shown in Fig. 5 is determined by the θ dependence of both ω_d and $k_\perp$. The mode is primarily localized near $\theta = 0$ in the bad curvature region. Landau damping is strongly

stabilizing for high $k_\parallel$, so the the most unstable modes have broad mode structures along the field line. Minimizing $k_\parallel$ while simultaneously localizing the modes in the bad curvature region leads to mode structures with $k_\parallel \approx 1/qR$, with large amplitude at the outer midplane and smaller amplitude at the inner midplane. Further along the field line (i.e. away from $\theta = 0$), magnetic shear causes $k_\perp$ to increase, which leads to FLR stabilization at large $\theta - \theta_0$. This magnetic shear stabilization through FLR effects keeps the mode amplitude small in bad curvature regions further along the field line, e.g. at $\theta = 2\pi$. When $\hat{s}$ or $k_\theta \rho_i$ are small, this magnetic shear effect is weaker, and the eigenfunctions become more extended in θ.

Fig. 6 compares the kinetic and fluid growth rates and real frequencies for the parameters of Fig. 3 in Ref. 32: $\eta_i = 1.5$, 2, and 3, $\epsilon_n = 0.2$, $q = 2$, $\hat{s} = 1$, and $\tau = 1$. The agreement between the 4+2 gyrofluid equations and kinetic theory is quite satisfactory, especially for $k_\theta \rho_i < 0.5$ where our models of FLR effects are very accurate. This level of agreement is a substantial improvement over previous fluid theories, and is more accurate than the four moment gyrofluid model of Ref. 8. As $k_\theta \rho_i$ decreases, the mode width increases and $k_\parallel$ becomes smaller. This shifts the long wavelength cutoff to lower $k_\theta \rho_i$ than in the local limit, where $k_\parallel$ is held fixed. In other respects the fully nonlocal results seem to follow the local trends fairly closely.

Fig. 7 shows a comparison with Fig. 4 of Ref. 32, using the parameters: $\eta_i = 2.5$, $\epsilon_n = 0.2$, 0.3, 0.45, $q = 1.5$, and $\hat{s} = 0.1 \times q/\epsilon_n$. The toroidal gyrofluid and kinetic results are not in terribly good agreement near marginal stability ($\epsilon_n = 0.45$), but for the agreement is satisfactory for $\epsilon_n = 0.2$ and 0.3.

To test of our models of trapped ion effects, we compare with the linear gyrokinetic particle simulations of Ref. 33, and the gyrokinetic "Vlasov" simulations of Ref. 34 which both include trapped ion effects. Fig. 8 shows a comparison of nonlocal linear eigenfrequencies from all three approaches, in the flat density limit, $\eta_i \to \infty$. The other parameters are: $L_T/R = 0.1$, $q = 2$, $\hat{s} = 1$, $\tau = 1$, and $\epsilon = 0.3$, in the collisionless limit, as in Fig. 6 of Ref. 33. All three calculations assumed adiabatic electrons. The gyrofluid and Vlasov results are shown both with ($\epsilon = 0.3$) and

without ($\epsilon = 0$) trapped ion effects, to show the destabilizing effect of the trapped ions for very long wavelengths. Since the $\nabla_\parallel \ln B$ mirroring terms are proportional to ϵ, setting $\epsilon = 0$ turns off these terms. Without the mirroring terms, all modes are stable below $k_\theta \rho_i \approx 0.04$. With the mirroring terms, the toroidal ITG mode gradually evolves into a trapped ion mode. Trapped ion effects become important when the mode time scales are comparable to or less than the ion bounce frequency, $|\omega| \lesssim \omega_{bi} = \sqrt{\epsilon} v_{ti}/qR$. For these parameters $\omega_{bi} L_T / v_{ti} = \sqrt{\epsilon} L_T / qR = 0.03$, so trapped ion effects become significant for $k_\theta \rho_i \lesssim 0.1$. The six moment toroidal gyrofluid equations model this effect with reasonable accuracy. In particular, the gyrofluid model shows that trapped ions can remove the long wavelength cutoff which exists when trapped ions are ignored, in agreement with fully kinetic theory.

In Fig. 9 we show the same results as in Fig. 8, but now normalized to v_{ti}/L_T, which is independent of k_θ, and is thus proportional to the growth rate in physical units. This demonstrates more clearly than in Fig. 8 that the growth rates of the trapped ion modes are much less than those of the fastest growing modes near $k_\theta \rho_i \sim 1/2$, and suggests that our models of trapped ion effects are probably adequate.

For the measured parameters used in Ref. 33, $\rho_i \approx 0.13$cm and $r_0 = 50$cm; so $k_\theta \rho_i = 0.01 = nq/r_0$ implies $n \approx 2$, where n is the toroidal mode number. Thus, the ballooning approximation is definitely breaking down at these very long wavelengths, and radial variations in the equilibrium will affect the mode structures and growth rates.

X. Summary and Discussion

In summary, we have derived toroidal ion gyrofluid equations with improved models of the important kinetic effects associated with toroidicity. Special care was taken to derive closure approximations which, though similar to those of Ref. 8, are well behaved in the mixed limit where both toroidal drifts and parallel free streaming are important, i.e. where both $k_\parallel$ and ω_d are non-zero. This work also extends the four moment toroidal gyrofluid model of Ref. 8 to six moments,

including the $\mu\hat{\mathbf{b}} \cdot \nabla B$ mirroring terms. By evolving six moments, no approximations are made to the parallel velocity equation, important for accurate poloidal flow damping rates. Including the $\mu\hat{\mathbf{b}} \cdot \nabla B$ terms also incorporates trapped ion effects to some extent; the growth rate in the very low $k_\theta \rho_i$ trapped ion mode regime is within a factor of two of fully kinetic calculations. The gyrofluid trapped ion results are in closer agreement with kinetic theory if we compare the diffusion ($\propto k_\perp^2 D$) required to stabilize the long wavelength trapped ion modes.[35] New toroidal FLR terms are treated which arise from the variation of B (in the argument of J_0) with major radius, and generalize the FLR model of Ref. 9 to toroidal geometry. An improved four moment model is also presented, which is simpler and numerically less demanding than the six moment model. Impurity and Maxwellian-model energetic particle dynamics are equally well described by these toroidal gyrofluid equations.

Although electrostatic turbulence effectively describes many experimental regimes, the electrostatic assumption is a limitation of the toroidal ion gyrofluid equations presented here. Recent work has begun including electromagnetic effects.[36,37] The main difficulty here is that magnetic fluctuations are driven by parallel current fluctuations, and since trapped particles do not carry current, passing electrons can no longer be considered adiabatic, and need to be evolved. Resolving the fast electron parallel motion seriously slows down the numerical calculations. Some trick analogous to bounce averaging, which is quite successful in simplifying the trapped electron dynamics,[7] would be useful for the passing electrons.

We conclude by discussing the validity of gyrofluid equations for plasma turbulence. These gyrofluid equations are an approximation to the full nonlinear gyrokinetic equation, and break down in some regimes. For example, in the slab limit, the weak turbulence wave-kinetic equation derived from the gyrofluid equations successfully reproduces the gyrokinetic wave-kinetic equation in the limit $\omega \gg k_\parallel v_{ti}$, but fails to recover the ion-Compton scattering rate very near marginal stability, in the limit $\gamma \ll \omega \ll k_\parallel v_{ti}$.[38,15] The nonlinear validity of the gyrofluid equations in strong turbulence regimes has not yet been unambiguously verified on fundamental grounds. However,

gyrofluid simulations have been compared against full gyrokinetic particle simulations, finding similar behavior full 3D sheared slab simulations and in three mode coupling test problems.[15,39] Toroidal simulations have also been benchmarked with toroidal gyrokinetic particle simulations, though not as extensively as the sheared slab simulations, and find reasonable agreement.[39] Very recently, the toroidal gyrokinetic particle simulations of Ref. 40 appear to predict lower transport by about a factor of 2. While in principle gyrokinetic simulations are more accurate, since they solve the gyrokinetic equation directly, there are a number of issues which need investigation: particle noise, particle filtering, resolution, and geometry (we implement field-line coordinates in a somewhat different way than Ref. 40, which tends to emphasize resolution in different parts of k-space). We have done some simulations with exactly the same particle filtering and box size as in Ref. 40, without magnetic shear ($\hat{s} = 0$) where our coordinate system and Ref. 40's coordinate system become identical. We then find that the gyrofluid simulation reproduces the gyrokinetic χ_i to within 20%. Turning off the particle filtering then causes χ_i to rise by a factor of 1.3, and our general experience is that increasing the box length in the parallel direction beyond 2π typically increases χ_i by a factor of 1.4. These resolution issues, and not intrinsic differences between the gyrofluid and gyrokinetic equations, thus appear to account for most of the differences seen so far, though more extensive comparisons would be worthy of eventual further study.

Another way to address the nonlinear accuracy of the linear closures is to consider a simple analytic model of the nonlinear terms, by using the renormalized kinetic equation. Here the nonlinear $\mathbf{v}_E \cdot \nabla f_1$ term in the linear kinetic equation is replaced by $\Delta\omega_{NL}\, f_1$:

$$(-i\omega + ik_\parallel v_\parallel + i\omega_d + \Delta\omega_{NL}) f_1 = (ik_\parallel v_\parallel e\Phi/T - \mathbf{v}_E \cdot \nabla) f_0.$$

This can now be integrated over velocity space to find a renormalized dispersion relation. If $\Delta\omega_{NL}$ is independent of velocity, this will be identical to the linear dispersion relation with ω replaced by $\omega + i\Delta\omega_{NL}$. This is sometimes used to determine a saturation level for the turbulence by requiring that $\Delta\omega_{NL}$ balance the linear growth rate. Closing the fluid hierarchy with linear closure

approximations naively appears to neglect $\Delta\omega_{NL}$ in the resonant denominator and appears to introduce an error of $\mathcal{O}(\Delta\omega_{NL}/k_\parallel v_{ti})$, which is typically $\mathcal{O}(1)$. However, the gyrofluid equations actually do much better than this. If we similarly renormalize the $\mathbf{E}\times\mathbf{B}$ nonlinearity in each gyrofluid equation and solve for the renormalized gyrofluid dispersion relation, we will obtain the three or four pole linear dispersion relation with ω again replaced by $\omega + i\Delta\omega_{NL}$. Thus the renormalized gyrofluid dispersion relation is just as good an approximation to the renormalized gyrokinetic dispersion relation as it was in the linear case. Of course there are many nonlinear processes which are not captured by this simple renormalized dispersion relation approximation, so this is not a proof that the gyrofluid closures always work nonlinearly. A novel discussion by Krommes and Hu[41] has addressed the correspondence between gyrofluid and gyrokinetic approaches to plasma turbulence in a very different way, by focusing on the role of dissipation in the two models.

More generally, each gyrofluid equation, as a moment of the gyrokinetic equation, is an exact nonlinear conservation law: closure approximations are introduced into higher moment equations in a way which preserves the conservative form the equations. Our equations retain the dominant ($\mathbf{E}\times\mathbf{B}$) nonlinearities and provide accurate physics based models of the linear drive and dissipation mechanisms. As more moments are retained, more details of the underlying distribution function are accurately described. In fact, Smith has demonstrated convergence in the number of moments for the nonlinear plasma echo problem,[11] though it required many moments in that case. In the strong turbulence limit, it seems unlikely that many moments need to be kept, since the broad spectrum of modes should average out sharp velocity space variations in the distribution function. Future work should continue to test the validity of the gyrofluid approximation, both through comparisons with kinetic simulations and through purely theoretical simplified problems.

References

[1]A. Hasegawa and K. Mima, Phys. Rev. Lett. **39**, 205 (1977).

[2]P. W. Terry and W. Horton, Phys. Fluids **25**, 491 (1982).

[3]R. E. Waltz, Phys. Fluids **29**, 3684 (1986).

[4]B. A. Carreras, L. Garcia, and P. H. Diamond, Phys. Fluids **30**, 1388 (1987).

[5]G. W. Hammett and F. W. Perkins, Phys. Rev. Lett. **64**, 3019 (1990).

[6]G. W. Hammett, W. Dorland, and F. W. Perkins, Phys. Fluids B **4**, 2052 (1992).

[7]M. A. Beer, Ph.D. thesis, Princeton University, 1995.

[8]R. E. Waltz, R. R. Dominguez, and G. W. Hammett, Phys. Fluids B **4**, 3138 (1992).

[9]W. Dorland and G. W. Hammett, Phys. Fluids B **5**, 812 (1993).

[10]M. A. Beer, S. C. Cowley, and G. W. Hammett, Phys. Plasmas **2**, 2687 (1995).

[11]G. W. Hammett, M. A. Beer, W. Dorland, S. C. Cowley, and S. A. Smith, Plasma Phys. Controlled Fusion **35**, 973 (1993).

[12]W. Dorland, M. Kotschenreuther, M. A. Beer, G. W. Hammett, R. E. Waltz, R. R. Dominguez, P. M. Valanju, W. H. Miner, J. Q. Dong, W. Horton, F. L. Waelbroeck, T. Tajima, and M. J. LeBrun, in *Plasma Physics and Controlled Nuclear Fusion Research, 1994* (International Atomic Energy Agency, Vienna, 1994), paper IAEA-CN-60/D-P-I-6.

[13]M. Kotschenreuther, W. Dorland, M. A. Beer, and G. W. Hammett, Phys. Plasmas **2**, 2381 (1995).

[14]W. Dorland, G. W. Hammett, T. S. Hahm, and M. A. Beer, Bull. Am. Phys. Soc. **37**, 1478 (1992).

[15]W. Dorland, Ph.D. thesis, Princeton University, 1993.

[16]M. A. Beer, G. W. Hammett, W. Dorland, and S. C. Cowley, Bull. Am. Phys. Soc. **37**, 1478 (1992).

[17]T. S. Hahm, Phys. Fluids **31**, 2670 (1988).

[18]E. A. Frieman and L. Chen, Phys. Fluids **25**, 502 (1982).

[19]W. W. Lee, Phys. Fluids **26**, 556 (1983).

[20]D. H. E. Dubin, J. A. Krommes, C. Oberman, and W. W. Lee, Phys. Fluids **26**, 3524 (1983).

[21]W. W. Lee, J. Comput. Phys. **72**, 243 (1987).

[22]A. Brizard, Phys. Fluids B **4**, 1213 (1992).

[23]E. P. Gross and M. Krook, Phys. Rev. **102**, 593 (1956).

[24]T. E. Stringer and J. W. Connor, Phys. Fluids **14**, 2177 (1971).

[25]P. Bakshi, W. Bellew, G. Ganguli, and P. Satyanarayana, presented at the 1977 Sherwood Theory Conference (unpublished).

[26]R. Linsker, Phys. Fluids **24**, 1485 (1981).

[27]J. Y. Kim, Y. Kishimoto, W. Horton, and T. Tajima, Phys. Plasmas **1**, 927 (1994).

[28]H. Biglari, P. H. Diamond, and M. N. Rosenbluth, Phys. Fluids B **1**, 109 (1989).

[29]J. Y. Kim and W. Horton, Phys. Fluids B **3**, 1167 (1991).

[30]W. H. Press, B. P. Flannery, S. A. Teukolsky, and W. T. Vetterling, *Numerical Recipes* (Cambridge University Press, Cambridge, 1986).

[31]G. F. Chew, M. L. Goldberger, and F. E. Low, Proc. Roy. Soc. **A236**, 112 (1956).

[32]J. Q. Dong, W. Horton, and J. Y. Kim, Phys. Fluids B **4**, 1867 (1992).

[33]X. Q. Xu and M. N. Rosenbluth, Phys. Fluids B **3**, 627 (1991).

[34]Q. P. Liu and C. Z. Cheng, Bull. Am. Phys. Soc. **38**, 2102 (1993).

[35]W. Dorland, private communication (unpublished).

[36]R. E. Waltz, G. D. Kerbel, J. Milovich, and G. W. Hammett, Phys. Plasmas **2**, 2408 (1995).

[37]G. W. Hammett, M. A. Beer, J. C. Cummings, W. Dorland, W. W. Lee, H. E. Mynick, S. E. Parker, R. A. Santoro, M. Artun, H. P. Furth, T. S. Hahm, G. Rewoldt, W. M. Tang, R. E. Waltz, G. D. Kerbel, and J. Milovich, in *Plasma Physics and Controlled Nuclear Fusion Research, 1994* (International Atomic Energy Agency, Vienna, 1994), paper IAEA-CN-60/D-2-II-1.

[38]N. Mattor, Phys. Fluids B **4**, 3952 (1992).

[39]S. E. Parker, W. Dorland, R. A. Santoro, M. A. Beer, Q. P. Liu, W. W. Lee, and G. W. Hammett, Phys. Plasmas **1**, 1461 (1994).

[40]A. M. Dimits, J. A. Byers, T. J. Williams, B. I. Cohen, X. Q. Xu, R. H. Cohen, J. A. Crotinger, and A. E. Shestakov, in *Plasma Physics and Controlled Nuclear Fusion Research, 1994* (International Atomic Energy Agency, Vienna, 1994), paper IAEA-CN-60/D-P-I-5.

[41]J. A. Krommes and G. Hu, Phys. Plasmas **1**, 3211 (1994).

List of Figures

1 Kinetic and fluid toroidal response functions in the purely toroidal limit, R_0, R_1, and R_2, with $b = 0$ and $k_\parallel = 0$. . . . . .

2 Kinetic and fluid toroidal response functions in the mixed toroidal/slab limit, R_0, R_1, and R_2, with $b = 0$ and $k_\parallel v_t/\omega_d = 2.7$. . . . . .

3 Comparison of local linear growth rates from the (4+2) and (3+1) toroidal gyrofluid equations vs. kinetic theory in the toroidal limit, with $k_\parallel = 0$ and $b = 0$. The four moment equations in Sec. VIII reproduce the stable low ϵ_n regime better than the four moment model in Ref. 4 but is slightly less accurate at large ϵ_n. The six moment equations are much more accurate, and are quite good for $\eta_i > 1$, away from marginal stability. . . . . .

4 Local growth rates from the six moment toroidal gyrofluid equations compared with kinetic theory, now in the mixed toroidal/slab limit with $k_\parallel = 0.1$ and $\epsilon_n = 0.2$. The toroidal gyrofluid equations again provide a very accurate model of the fully kinetic results. . . . . .

5 Linear nonlocal eigenfunction comparison with the fully kinetic calculations of Ref. 26. The coordinate along the field line, θ, is equivalent to the "extended ballooning angle." . . . . .

6 Nonlocal linear growth rate and real frequency comparison between the toroidal gyrofluid equations and kinetic theory, for the four moment and six moment models. The six moment model provides excellent agreement with fully kinetic theory, especially for $k_\theta \rho_i < 1/2$. . . . . .

7 Comparison of linear growth rates from kinetic theory and the six moment model. Again, the agreement is quite good except for $\epsilon_n = 0.45$, where $\hat{s} = 1/3$. . . . . .

8 Comparison of linear growth rates and real frequencies normalized to $\omega_* T$ from fully kinetic calculations and the six moment toroidal gyrofluid equations with trapped ion effects. Including trapped ions ($\epsilon = 0.3$) further destabilizes the toroidal ITG mode at long wavelengths, which gradually evolves into a trapped ion mode for $k_\theta \rho_i \lesssim 0.1$.

9 Linear growth rates and real frequencies normalized to v_t/L_T. In physical units, the growth rates of the trapped ion modes are much less than those of the fastest growing modes near $k_\theta \rho_i \sim 1/2$, which suggests that our models of trapped ion effects are probably adequate. . . . . .

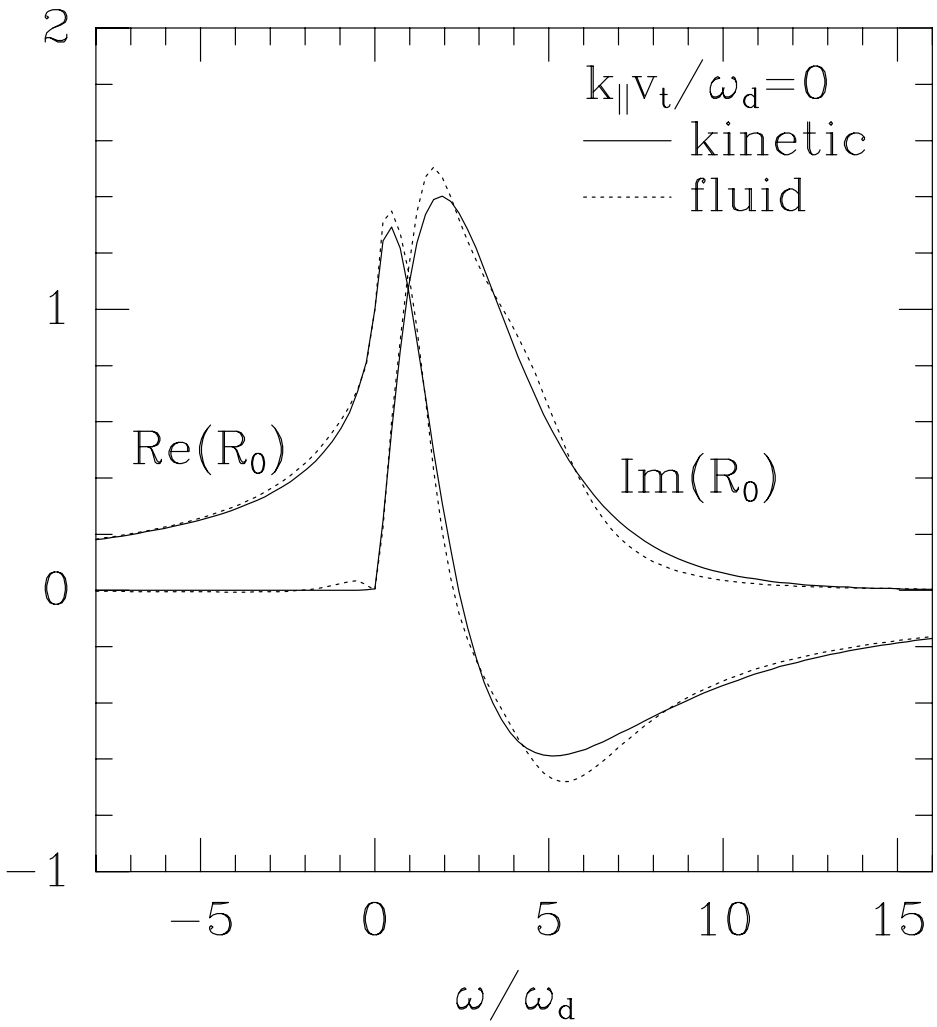
2
1
0
−1
−5
0
5
10
15
$k_{||}v_t/\omega_d=0$
kinetic
fluid
$\mathrm{Re}(R_0)$
$\mathrm{Im}(R_0)$
ω/ω_d

Figure 1: (a)

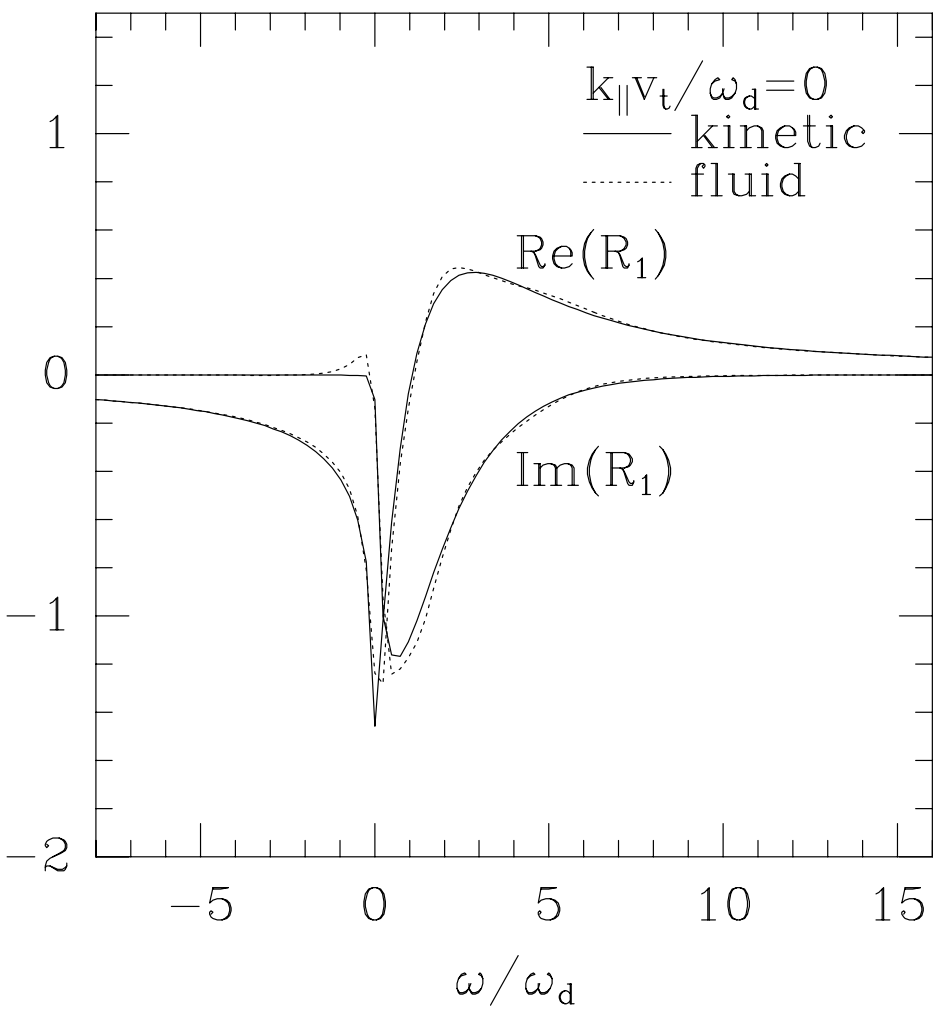
$k_{||}v_t/\omega_d=0$
kinetic
fluid
$\mathrm{Re}(R_1)$
$\mathrm{Im}(R_1)$
1
0
−1
−2
−5
0
5
10
15
ω/ω_d

Figure 1(b)

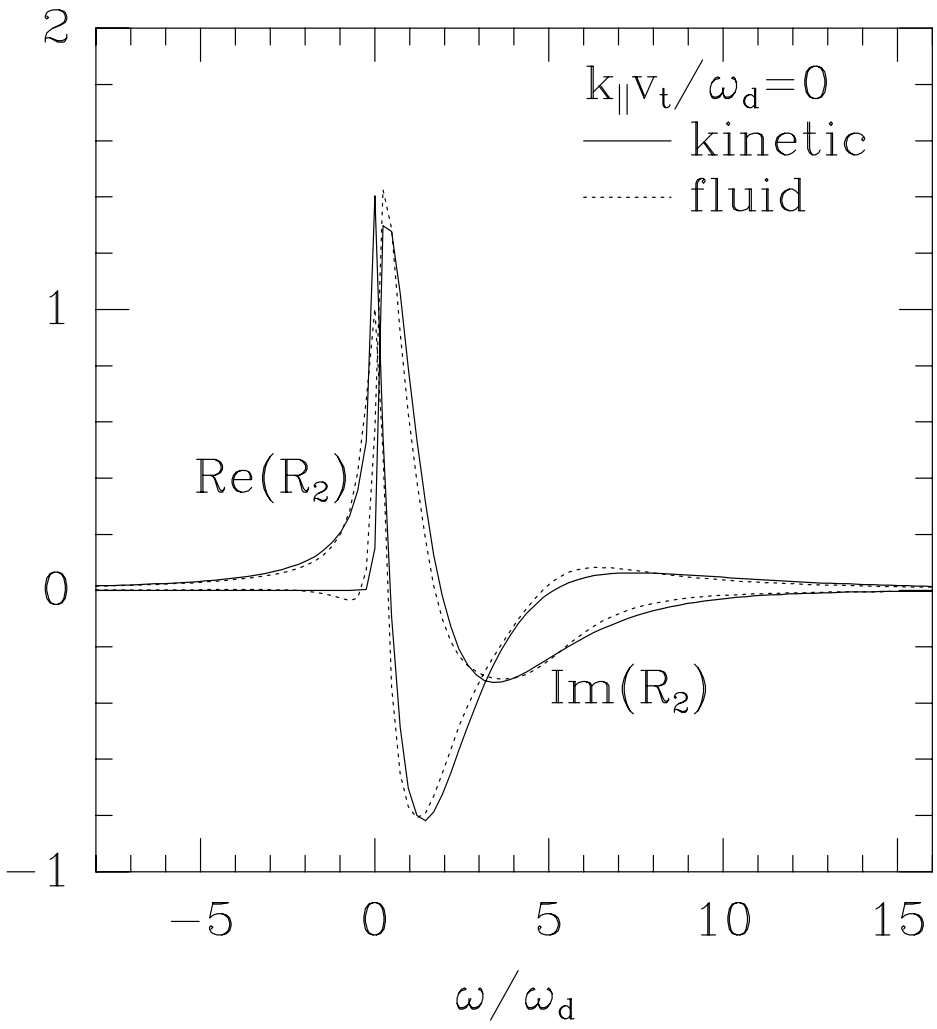
2
1
0
−1
−5
0
5
10
15
$k_{||}v_t/\omega_d=0$
kinetic
fluid
$\mathrm{Re}(R_2)$
$\mathrm{Im}(R_2)$
ω/ω_d

Figure 1(c)

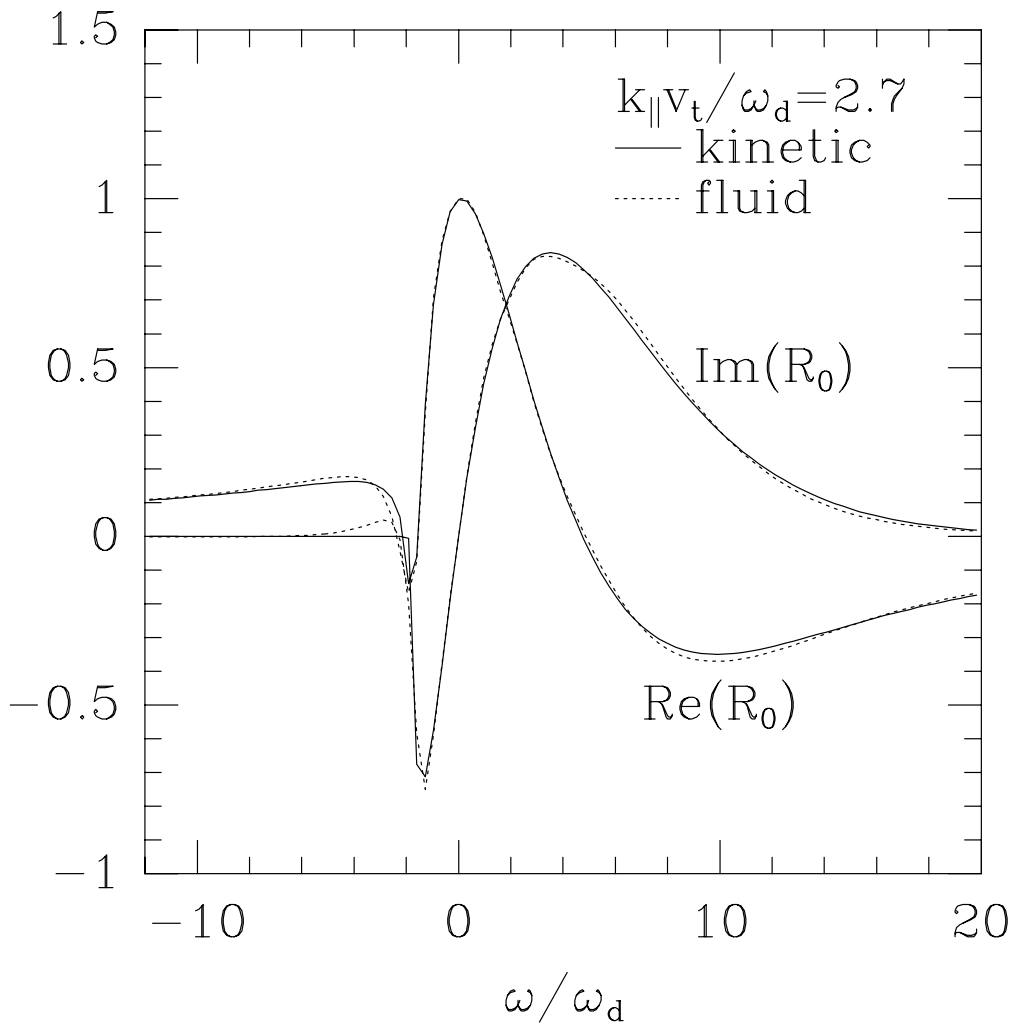
1.5
1
0.5
0
−0.5
−1
−10
0
10
20
$k_\parallel v_t/\omega_d$=2.7
kinetic
fluid
Im(R_0)
Re(R_0)
ω/ω_d

Figure 2: (a)

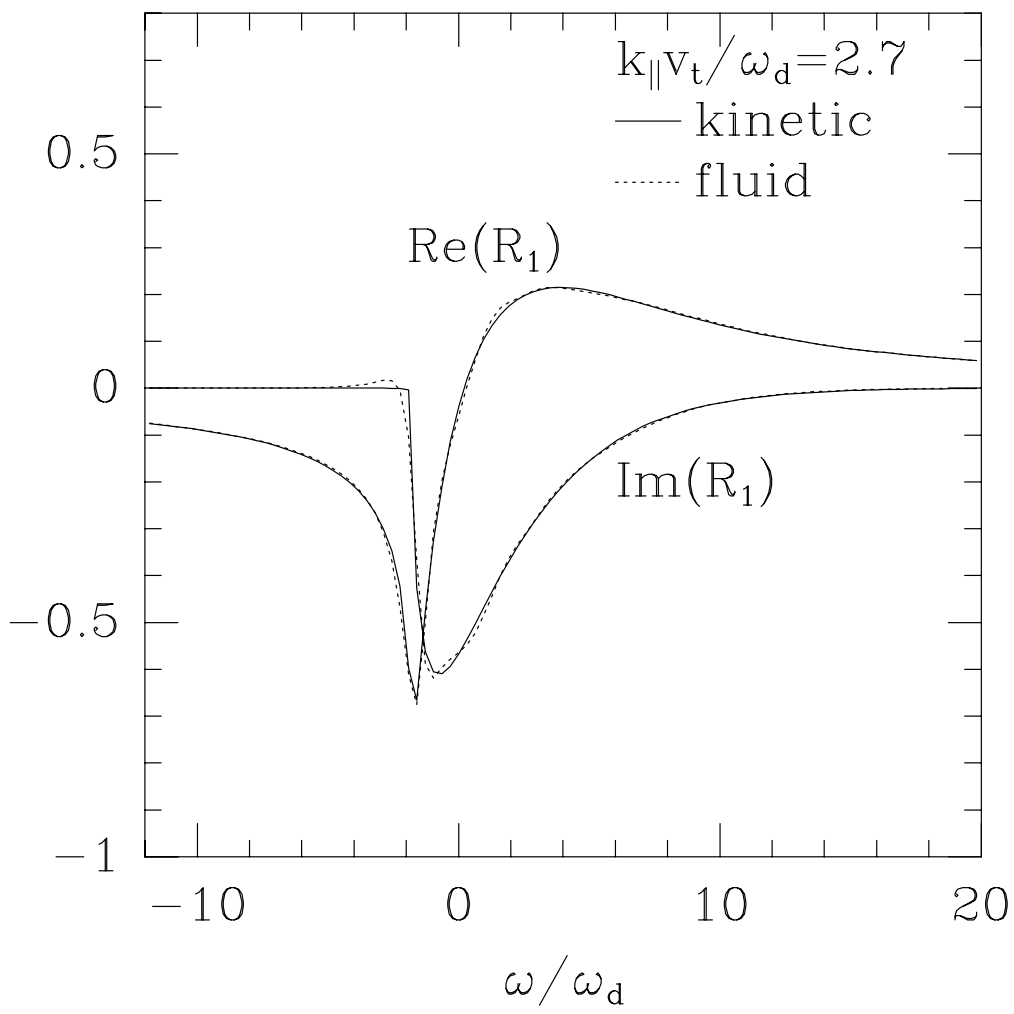
$k_{\|}v_t/\omega_d$=2.7
kinetic
fluid
Re(R_1)
Im(R_1)
0.5
0
−0.5
−1
−10
0
10
20
ω/ω_d

Figure 2(b)

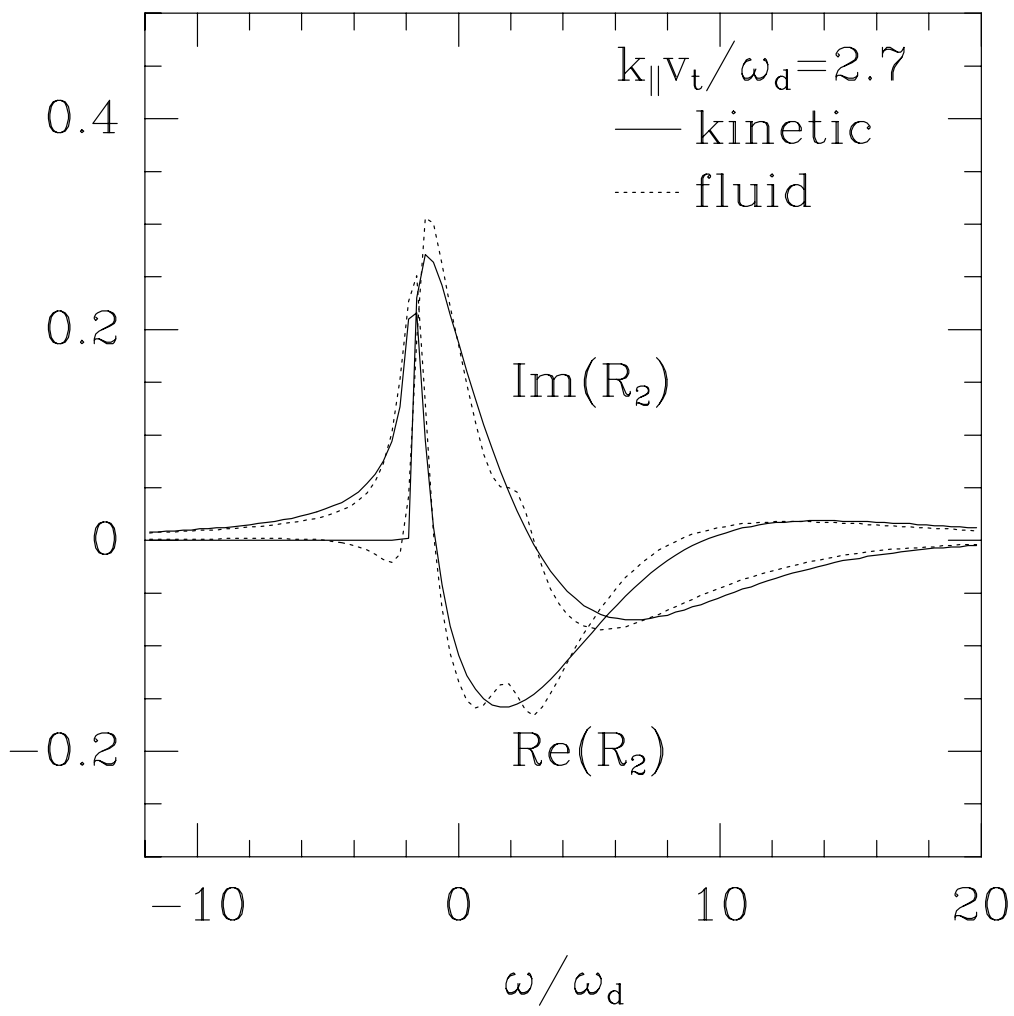
$k_\parallel v_t/\omega_d$=2.7
kinetic
fluid
Im(R_2)
Re(R_2)
0.4
0.2
0
−0.2
−10
0
10
20
ω/ω_d

Figure 2(c)

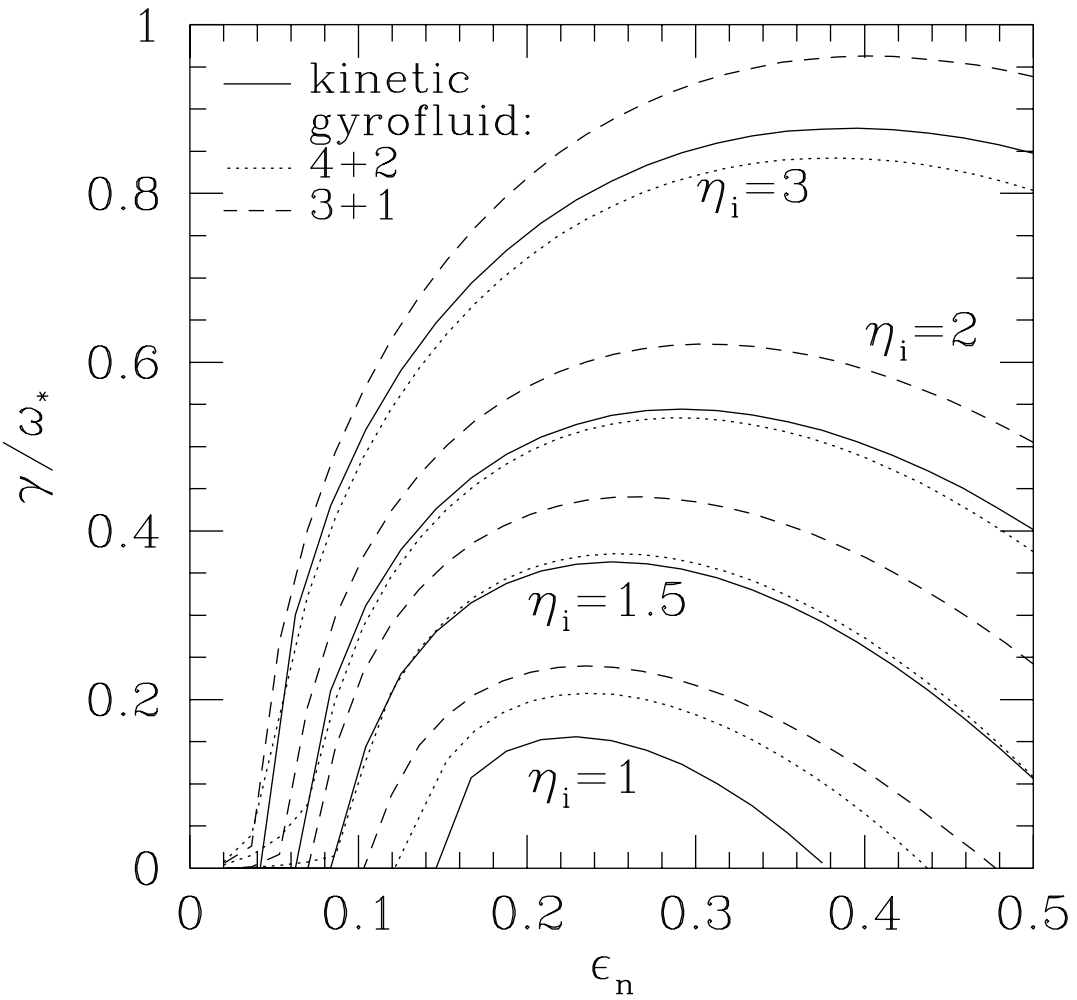
kinetic
gyrofluid:
4+2
3+1
η_i=3
η_i=2
η_i=1.5
η_i=1
γ/ω_*
ϵ_n
0
0.2
0.4
0.6
0.8
1
0.1
0.3
0.5

Figure 3:

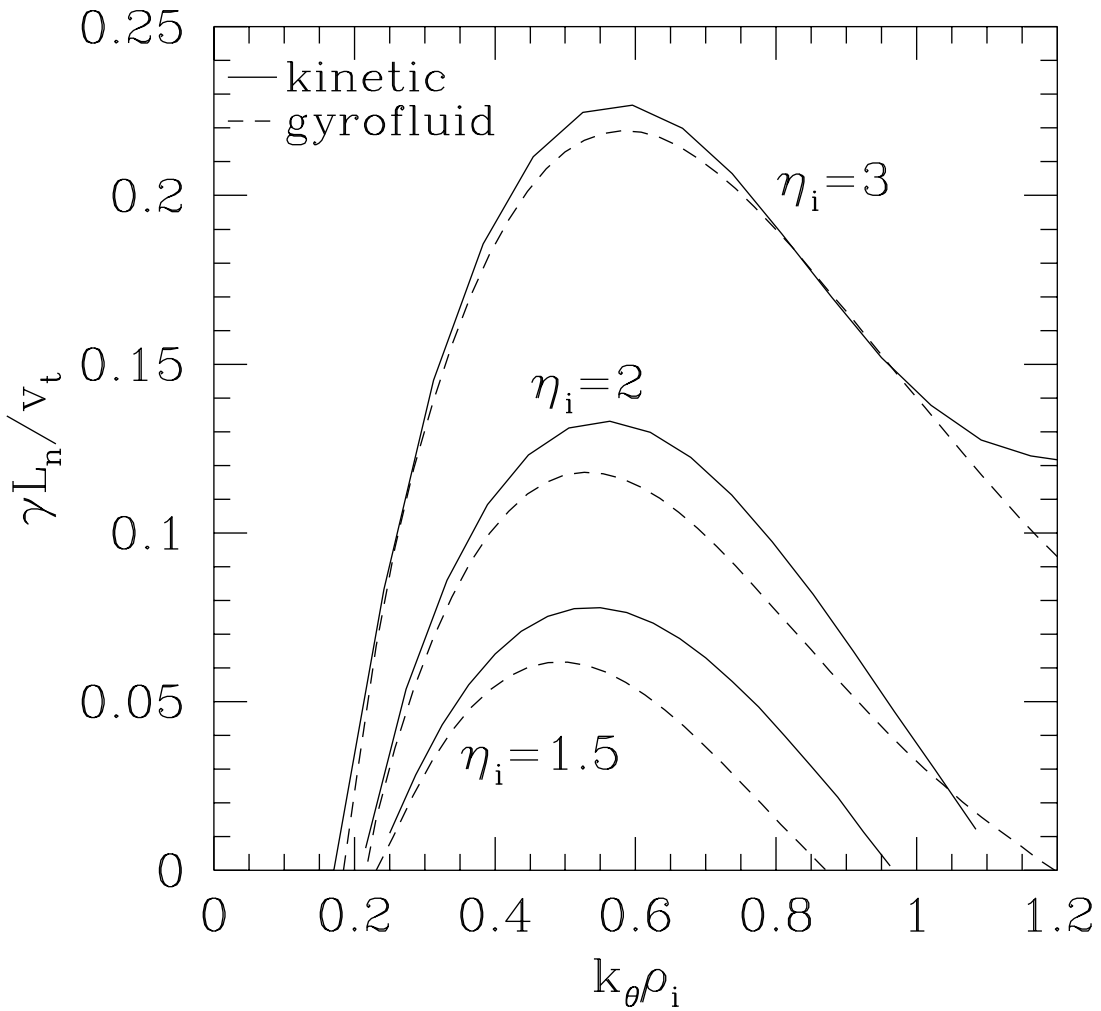
0.25
0.2
0.15
0.1
0.05
0
kinetic
gyrofluid
η_i=3
η_i=2
η_i=1.5
$\gamma L_n / v_t$
0
0.2
0.4
0.6
0.8
1
1.2
$k_\theta \rho_i$

Figure 4:

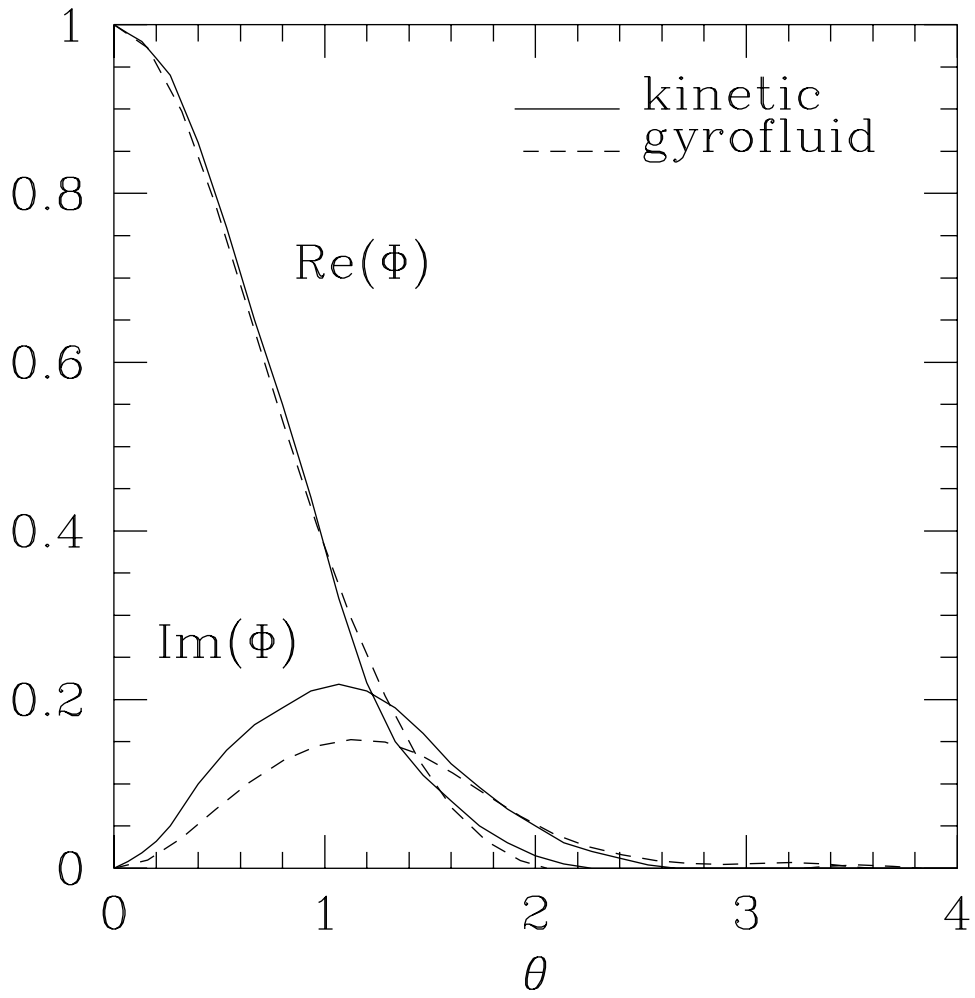

Figure 5:

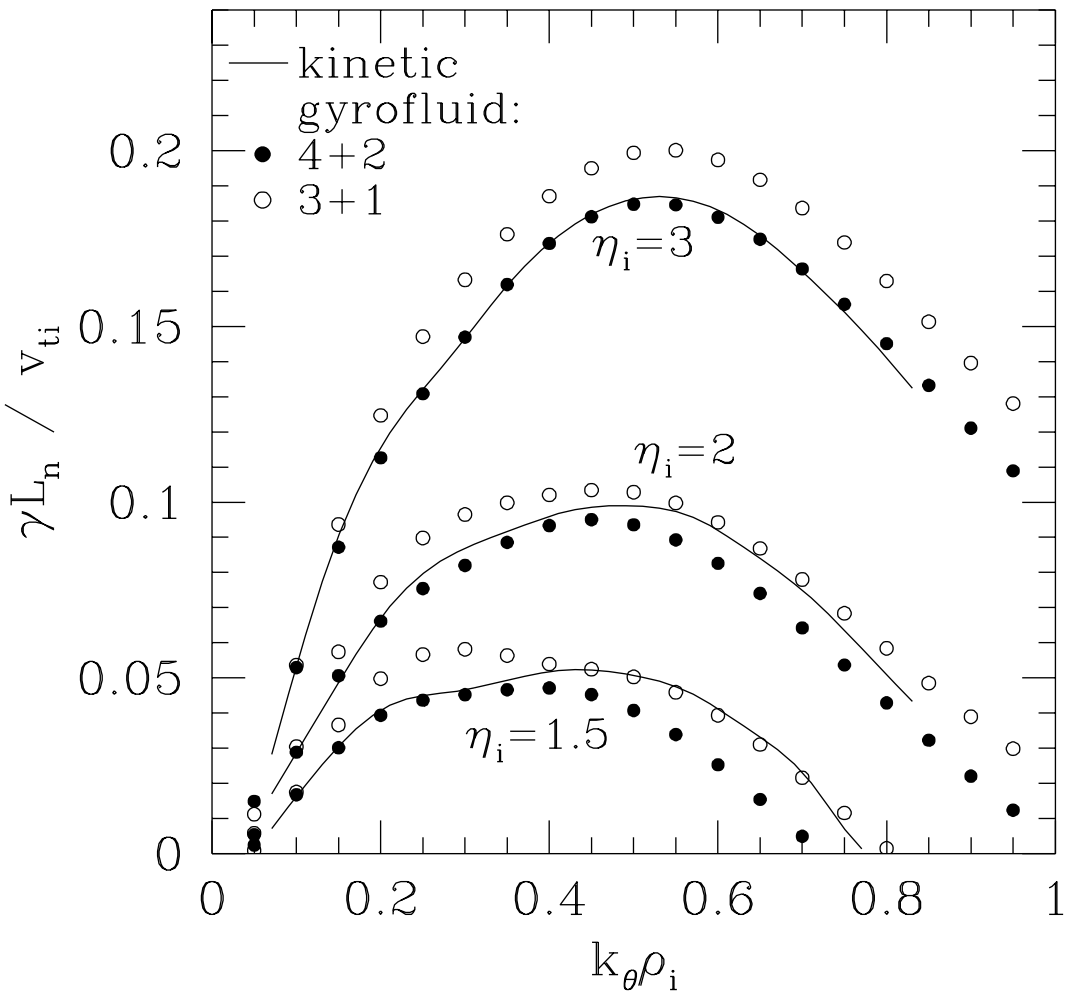
kinetic
gyrofluid:
4+2
3+1
η_i=3
η_i=2
η_i=1.5
γL_n / v_{ti}
$k_\theta \rho_i$
0
0.05
0.1
0.15
0.2
0.2
0.4
0.6
0.8
1

Figure 6: (a)

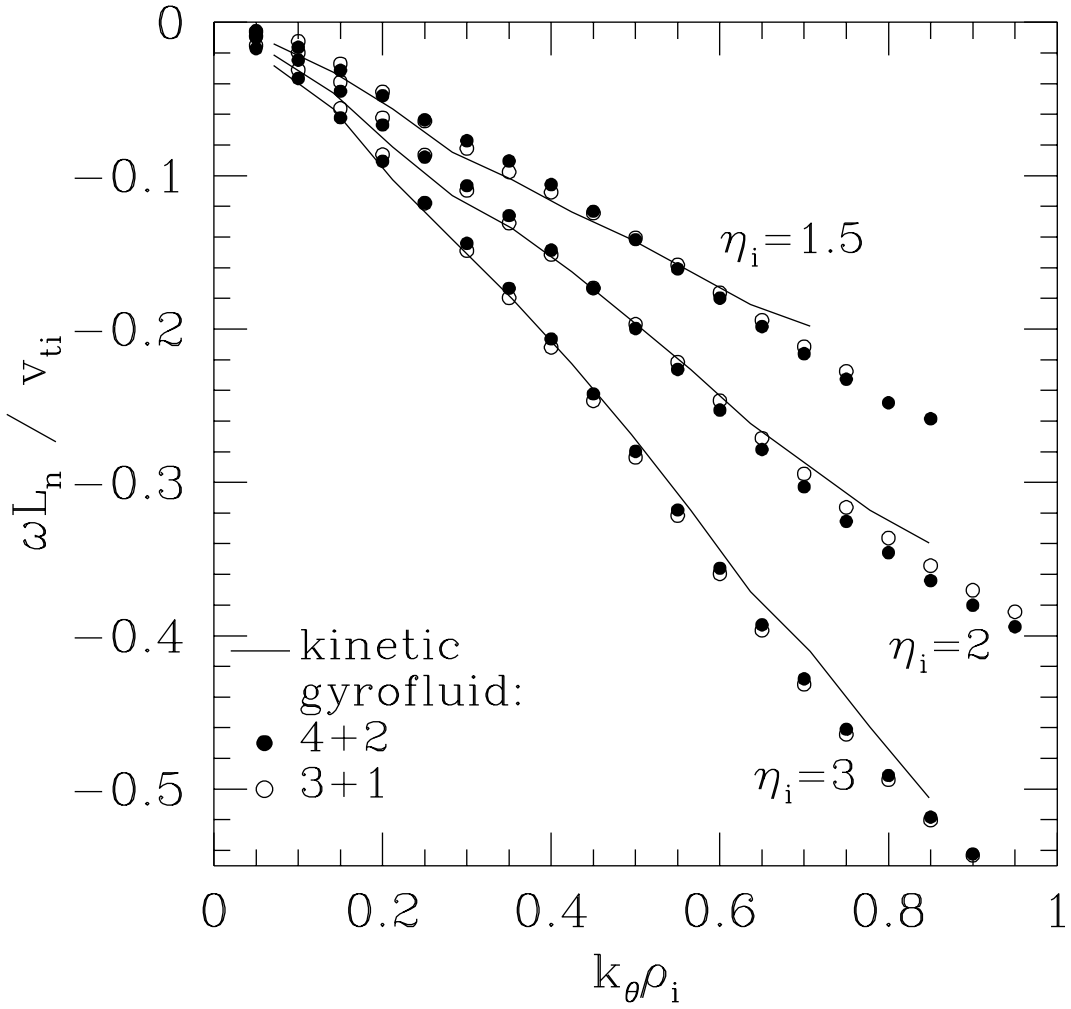
0
−0.1
−0.2
−0.3
−0.4
−0.5
ω L_n / v_ti
kinetic
gyrofluid:
4+2
3+1
η_i=1.5
η_i=2
η_i=3
0
0.2
0.4
0.6
0.8
1
k_θ ρ_i

Figure 6(b)

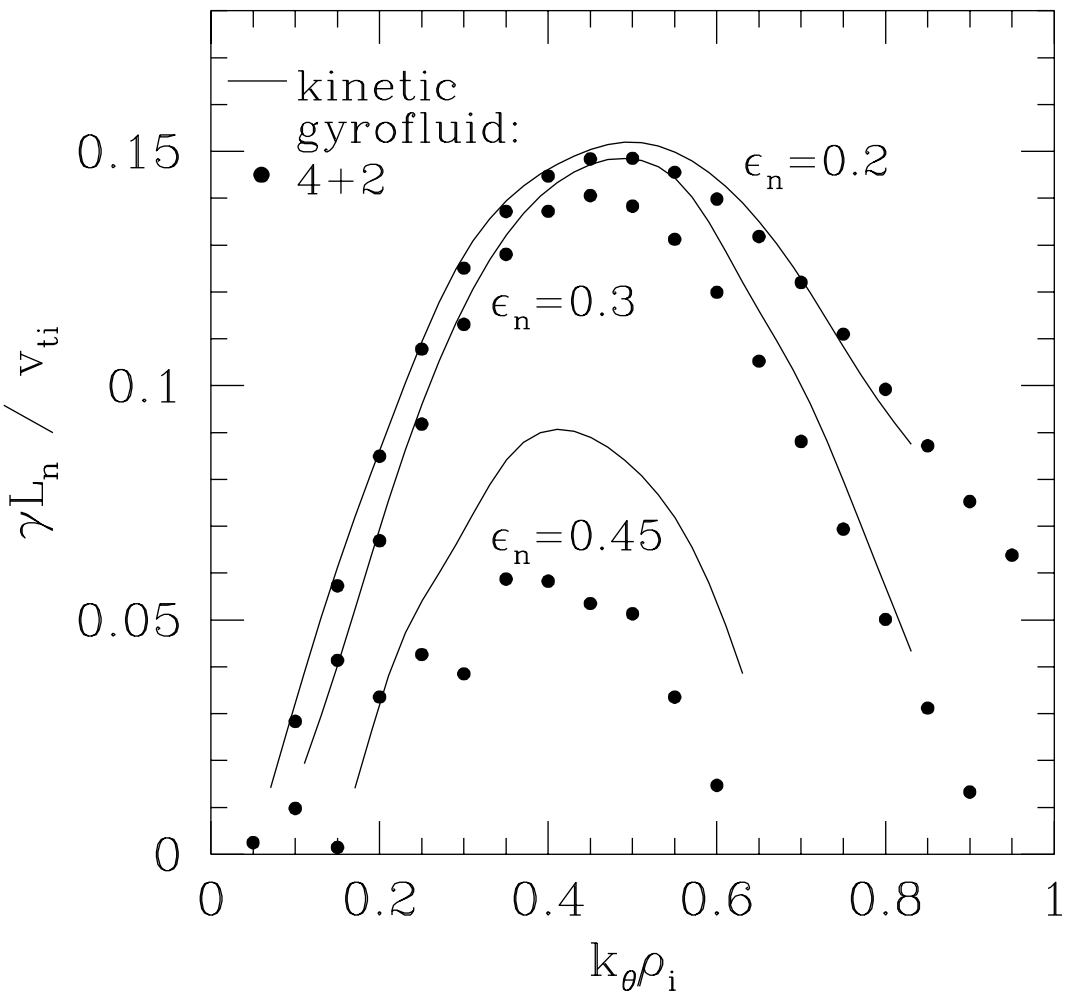
kinetic
gyrofluid:
4+2
ϵ_n=0.2
ϵ_n=0.3
ϵ_n=0.45
$\gamma L_n / v_{ti}$
$k_\theta \rho_i$
0
0.05
0.1
0.15
0.2
0.4
0.6
0.8
1

Figure 7:

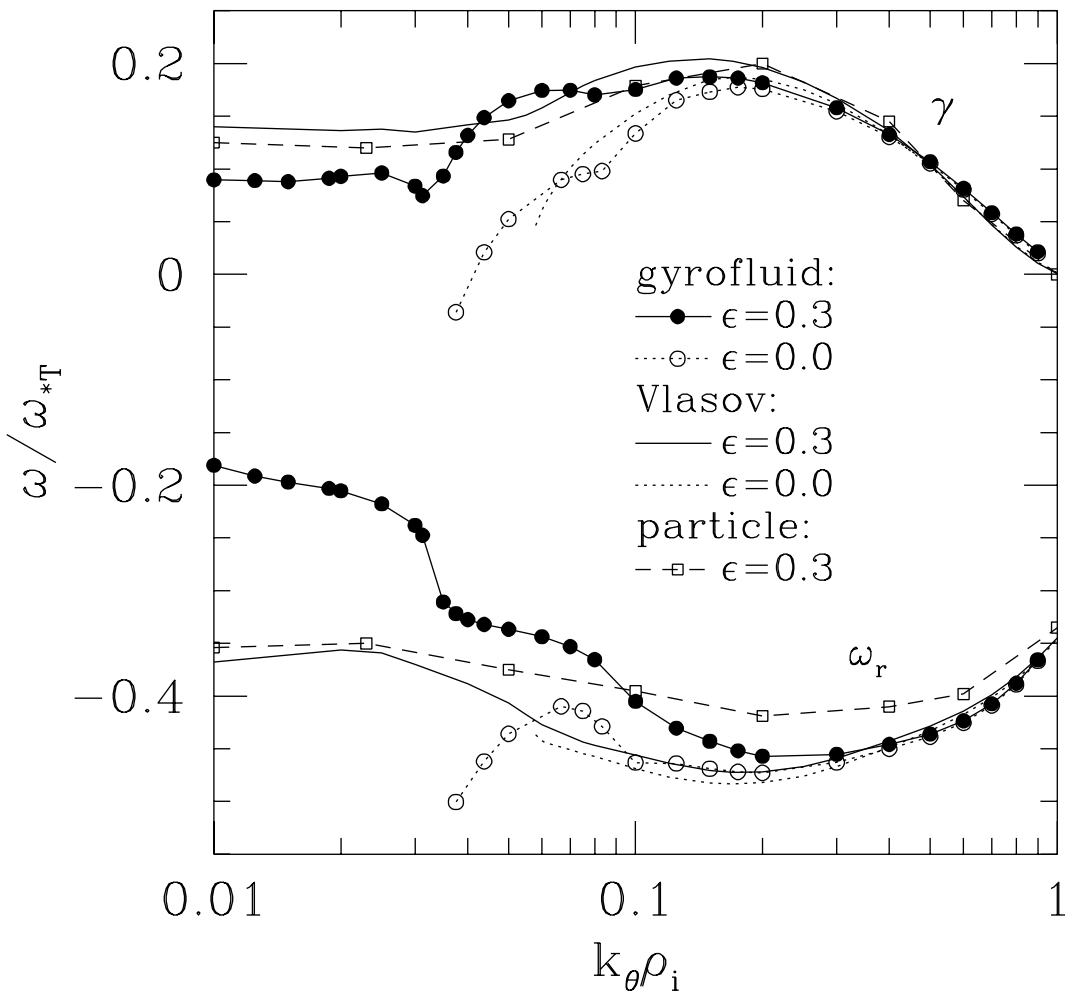
0.2
0
−0.2
−0.4
ω/ω*T
0.01
0.1
1
k_θρ_i
γ
ω_r
gyrofluid:
ϵ=0.3
ϵ=0.0
Vlasov:
ϵ=0.3
ϵ=0.0
particle:
ϵ=0.3

Figure 8:

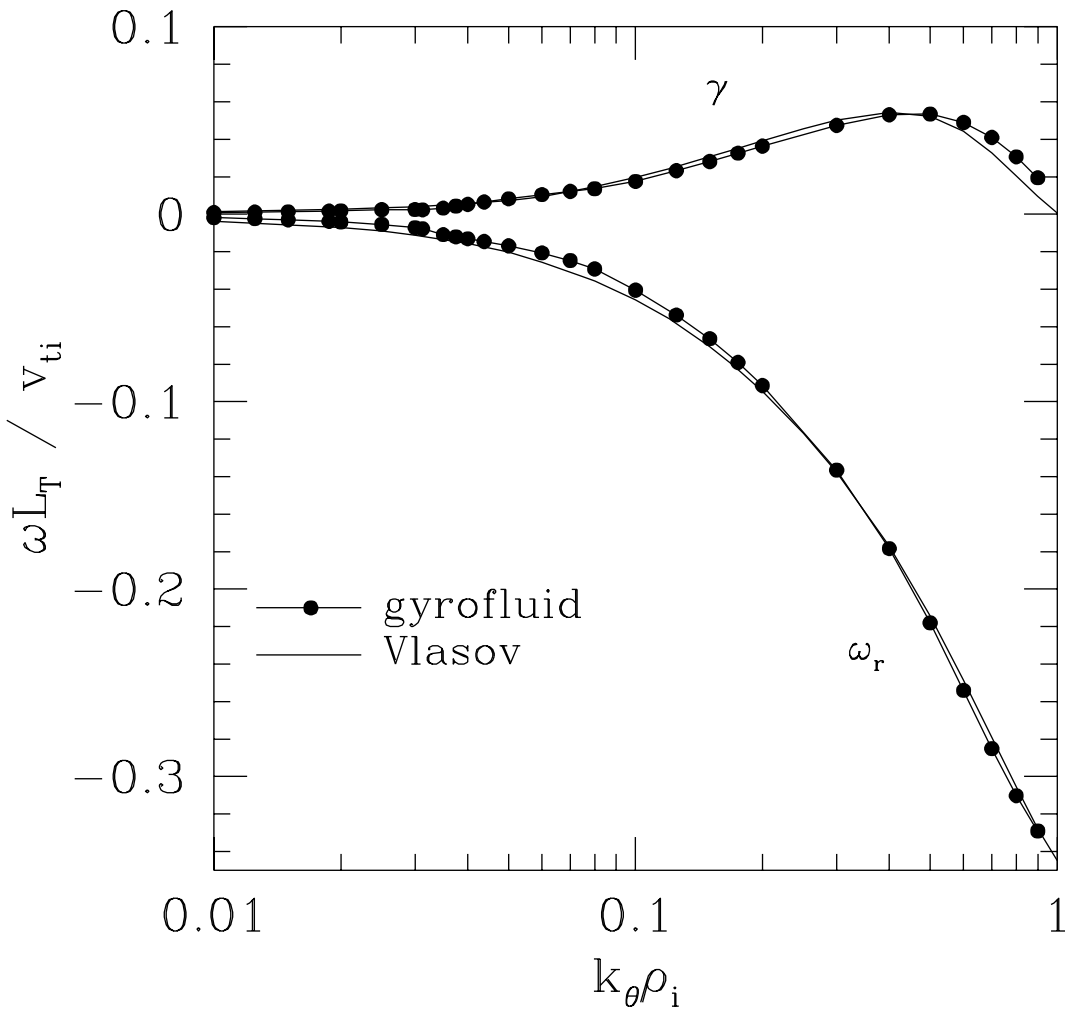
0.1
0
−0.1
−0.2
−0.3
0.01
0.1
1
$\omega L_T / v_{ti}$
$k_\theta \rho_i$
γ
ω_r
gyrofluid
Vlasov

Figure 9: